WCAP-10514, Vol 1
DOE/ET 34014-14 - Vol. 1

UC-78

## DISCLAIMER



# HOT CELL EXAMINATION OF SURRY THREE- AND FOUR-CYCLE 17x17 DEMONSTRATION FUEL VOLUME 1 PRINCIPAL RESULTS AND EVALUATION

DOE/ET/34014--14-Vol.1
DE84 015871

J. A. Kuszyk

June 1984

Approved: W. F. Staley
W. F. Staley,
Program Manager

Approved E. Roberts for
E. Roberts
Manager, Materials
Analysis & Development

Prepared under subcontract to
Virginia Electric and Power Company

under

United States Department of Energy
Prime Contract No. DE-AOC2-79ET34014

by

WESTINGHOUSE ELECTRIC CORPORATION
Nuclear Energy Systems
P.O. Box 355
Pittsburgh, Pennsylvania 15230

---

## DISCLAIMER

## ABSTRACT

A comprehensive hot cell examination has been performed on 12 17x17 fuel rods irradiated in the Surry reactors. Four of the fuel rods had achieved an average burnup of 29,600 MWD/MTU over three cycles of irradiation in the demonstration assembly RD-2 which was irradiated in Surry Unit 2. Six of the fuel rods were irradiated over four cycles in the RD-2 assembly to an average burnup of 44,000 MWD/MTU. The remaining two rods examined in the program were of a lower initial enrichment and had substantially different power histories. These latter rods were irradiated in the Surry Unit 1 reactor in the RD-1 demonstration assembly for the first two cycles, after which they were transfered to the RD-2 assembly. The average burnup of these two rods over four cycles was 39,800 MWD/MTU.

The hot cell nondestructive and destructive examinations were undertaken at the Battelle Columbus Laboratories, West Jefferson, Ohio.

Based upon the hot cell examination, the Surry fuel rods showed no evidence of any significant materials limitations in achieving extended burnups to about 45,000 MWD/MTU.

## ACKNOWLEDGMENTS

Appreciation is extended to the following individuals for their contribution to this report:

- Dr. R. Kohli, Mr. V. Pasupathi, Battelle, Columbus, hot cell staff, for the destructive and nondestructive examinations
- S. Cecconie for helping with the computerized data reduction
- N. Croasdaile for her assistance in the compilation of the report
- Members of the Program Steering Committee for general program guidance

TABLE OF CONTENTS
VOLUME 1

TABLE OF CONTENTS (cont)
VOLUME 1

LIST OF ILLUSTRATIONS

LIST OF ILLUSTRATIONS (cont)

LIST OF TABLES

# SECTION 1
# INTRODUCTION

## 1-1. BACKGROUND

Previous government policy decisions which indefinitely deferred reprocessing and closure of the nuclear fuel cycle have increased the importance of demands placed on spent fuel storage and disposal facilities. The DOE Extended Burnup Program responds directly to this need by providing a technical basis for reducing the quantity of spent fuel which must be treated. This reduction would facilitate schedular changes in implementing the reprocessing and waste disposal functions. Extended burnup fuel management methods also provide significant improvements in uranium ore utilization for increases in region average discharge burnup above the present 33,000-36,000 MWD/MTU level.

The United States Department of Energy (DOE), the Virginia Electric and Power Company (VEPCO), and the Westinghouse Electric Corporation (WEC) are cooperating in an Extended Burnup Demonstration Program to study the feasibility of increasing the region average discharge burnup of PWR fuel assemblies to values exceeding 40,000 MWD/MTU as part of the normal fuel cycle. Under the agreement, VEPCO is the prime contractor and Westinghouse the principal subcontractor in implementing the program. The extended burnup program originally was divided into two major areas: (1) generic technical studies, which investigated the feasibility of extended fuel burnup in the areas of nuclear design, safety and licensing analysis, fuel management schemes, and related fuel cycle services; and (2) fuel performance data acquisition, to obtain performance data through nondestructive and destructive examination of an extended burnup 17x17 demonstration fuel assembly operated in the Surry Unit 2 reactor.

The data acquisition phase of the program involved irradiating a Westinghouse 17x17 demonstration assembly for a fourth irradiation cycle in the VEPCO Surry Unit 2 reactor. Irradiation in the fourth cycle began on August 14, 1980; the

assembly had attained a burnup of 42,511 MWD/MTU at the end of the irradiation cycle on November 7, 1981. Onsite nondestructive examinations were performed before and after the irradiation cycle, and destructive hot cell examinations were conducted on removable fuel rods from the discharged assembly. The results of these hot cell examinations are the subject of this report.

Details of onsite nondestructive examinations prior to the fourth assembly irradiation cycle (fifth reactor cycle) of removable fuel rod assembly RD-2 in the VEPCO Surry Unit 2 reactor have been reported.[1,2] The onsite examination following the fourth irradiation cycle is reported in WCAP-10317.[3] The onsite examinations of fuel assembly RD-2 are summarized in table 1-1, along with test information on the selected rods for hot cell examination.

A summary of the irradiation history of the 12 removable fuel rods selected for the hot cell examination is presented in table 1-2. Of the 12 rods, 10 were irradiated in Surry Unit 2, assembly RD-2, for either three or four cycles and had an enrichment of 3.10 percent U-235. The other two rods, with an enrichment of 1.85 percent U-235, had a slightly different power history because of their initial irradiation in Surry Unit 1, assembly RD-1, for two cycles prior to transfer to Unit 2, assembly RD-2, for an additional two cycles. All 12 rods were nondestructively examined at the hot cells; they were selected principally to maximize the range of burnup and rod average power conditions evaluated. The selection for destructive investigation, one three-cycle rod and three four-cycle rods, was made so that the effects of burnup and power level on the 17x17 fuel performance could be fully evaluated. A complete listing of the power and burnup history of the individual removable fuel rods can be found in Volume 2 of WCAP-10317.[3]

## 1-2. HOT CELL EXAMINATION OBJECTIVES

The primary objective of the postirradiation hot cell examination program was to verify the ability of the fuel rods to sustain high burnup. Specific items of interest for both three- and four-cycle removable rods were as follows:

# TABLE 1-1

## SUMMARY OF EXPOSURE AND ONSITE EXAMINATION OPERATIONS FOR FUEL RODS FROM SURRY UNIT 2, ASSEMBLY RD-2

| EXPOSURE DATA | Unit 1, Assembly RD-1 | | Unit 2, Assembly RD-2 | | | | | | | | | | | |
|---|---|---|---|---|---|---|---|---|---|---|---|---|---|---|
| Rod number | 888 | 888 | 888 | 888 | 501 | 502 | 507 | 509 | 511 | 512 | 513 | 515 | 889 | 889 |
| Grid cell | E-9 | M-11 | E-9 | M-13 | I-10 | E-13 | H-10 | I-8 | I-13 | E-5 | H-8 | M-5 | M-9 | D-7 |
| w/o U-235 | 1.85 | 1.85 | 1.85 | 1.85 | 3.10 | 3.10 | 3.10 | 3.10 | 3.10 | 3.10 | 3.10 | 3.10 | 3.10 | 3.10 |
| Reactor cycles | 2,3 | 2,3 | 4,5 | 4,5 | 2-5 | 2-5 | 2-4 | 2-5 | 2-5 | 2-5 | 2-5 | 2-4 | 2-4 | 2-4 |
| Exposure cycles | 2 | 2 | 2 | 2 | 4 | 4 | 3 | 4 | 4 | 4 | 4 | 3 | 3 | 3 |
| EOC-2, GWD/MTU | 8.0 | 8.2 | - | - | 8.1 | 9.1 | 9.2 | 8.1 | 8.0 | 9.1 | 9.2 | 6.3 | 6.3 | 9.1 |
| EOC-3, GWD/MTU | 16.9 | 17.5 | - | - | 15.2 | 14.6 | 15.7 | 15.2 | 15.0 | 14.6 | 14.7 | 14.6 | 14.6 | 14.0 |
| EOC-4, GWD/MTU | - | - | 28.4 | 28.7 | 30.7 | 29.7 | 29.6 | 30.6 | 30.4 | 29.7 | 29.6 | 30.0 | 30.0 | 28.9 |
| EOC-5, GWD/MTU | - | - | 39.6 | 40.0 | 44.3 | 43.8 | - | 44.5 | 44.3 | 43.9 | 43.4 | - | - | - |
| Discharged at EOC- | 3 | 3 | 5 | 5 | 5 | 5 | 4 | 5 | 5 | 5 | 5 | 4 | 4 | 4 |
| EXAMINATION OPERATIONS Item | Performed At End of Indicated Cycle | | | | | | | | | | | | | |
| Detailed TV visual | 2 | 2 | 5 | 5 | 2,4,5 | 2,4,5 | 2 | 2,4,5 | 2,4,5 | 2,4,5 | 5 | 2 | 2 | |
| Cursory TV visual | | | 4 | 4 | | | 4 | | | | | 4 | 4 | |
| Breakaway and withdrawal force | 2,3 | 2,3 | 5 | 5 | 2,4,5 | 2,4,5 | | 2,4,5 | 2,4,5 | 2,4,5 | 5 | 2 | 2 | |
| Grid cell friction force | | | 4,5 | 4,5 | | 4,5 | | 5 | 4,5 | 4,5 | 5 | | | |
| Profilometry | | | | | 4 | 2,4 | | 4 | 2,4 | 4 | | 2 | | |
| Fuel stack length | | | | | 2 | 2 | | 2 | 2 | 2 | | 2 | | |

TABLE 1-2

SUMMARY OF IRRADIATION HISTORY OF REMOVABLE FUEL RODS
SELECTED FOR HOT CELL EXAMINATION

| Irradiation History | Number of Rods | Initial Enrichment (w/o U-235) | Rod Average EOL Burnup Range (GWD/MTU) | Rod Average Operating Power Range (kw/ft) | Number of Rods Examined | |
|---|---|---|---|---|---|---|
| | | | | | Nondestructive | Destructive |
| 3 cycles (Surry Unit 2, RD-2) | 4 | 3.10 | 29-30 | 3.1-5.4 | 4 | 1 |
| 4 cycles (Surry Unit 2, RD-2) | 6 | 3.10 | 43-44 | 3.1-5.4 | 6 | 3 |
| 4 cycles (2 cycles, Surry Unit 1, RD-1; then 2 cycles Surry Unit 2, RD-2) | 2 | 1.85 | 40 | 4.8-5.9 | 2 | 1 |

- Visual examination of rods to characterize their surface for the distribution and nature of crud deposits and the Zircaloy oxide corrosion layer

- Hot cell diametral profilometry evaluation, focusing on clad creep, ridging, ovality, and rod and pellet stack length measurement

- Fission gas composition and internal volume data evaluation to determine fractional fission gas release as a function of burnup and power history

- Fuel and clad metallographic evaluation for fuel grain size, density, and pore distribution; fuel to clad bonding; clad oxide thickness; and clad hydride orientation

- Determination of clad hydrogen uptake as a function of burnup

- Examination of fuel and cladding samples to verify fuel burnup and clad fast fluence values previously calculated from core operational follow data

## 1-3. HOT CELL WORK SCOPE

In the assessment of assembly RD-2 fuel rod performance, both nondestructive and destructive examination of the fuel rods, cladding, and fuel pellets were included. The overall work scope at the Battelle Columbus Laboratories (BCL) hot cells is presented in table 1-3.

TABLE 1-3

ACTIVITIES CONDUCTED AT BCL

| Activity | Number of Rods/Samples | |
|---|---|---|
| | 3-Cycle | 4-Cycle |
| Visual examination | 4 | 8 |
| Gamma scan | 4 | 8 |
| Profilometry | 4 | 8 |
| Oxide thickness | 4 | 8 |
| Length | 4 | 8 |
| Fission gas analysis | 4 | 8 |
| Fuel and clad metallography | 2 samples | 7 samples |
| Density | 2 | 2 |
| Burnup analysis | 2 | 2 |
| $H_2$ and Mn-54 analysis | 3/2 | 6/2 |

# SECTION 2
# FUEL ASSEMBLY AND FUEL ROD CHARACTERISTICS AND ROD FABRICATION

The basic characteristics of the fuel rods which constituted fuel assembly RD-2 have been detailed. The essential features of the assembly and fuel rods are presented in appendix A of this report. Appendix A includes information on the basic design and fabrication of RD-2, along with the fuel rod loading and fuel assembly core location history. A general description of the cladding and fuel pellets is also included.

The most pertinent as-built characteristics of removable fuel rods in assembly RD-2 are presented in appendix B of this report. Appendix B contains information on the fuel rod fabrication procedure, along with preirradiation data on rod length, rod outside diameters, rod bow, plenum lengths, fuel stack continuity, fuel column lengths, and rod pressurization.

# SECTION 3
# CASK AND FUEL HANDLING

This section briefly summarizes the transfer of the fuel rods selected for this hot cell examination program from the Surry site to the Battelle Columbus Laboratories (BCL), West Jefferson, Ohio, hot cell site.

The 12 fuel rods were transported in a fuel rod shipping basket (FRSB) designed by Nuclear Assurance Corporation to be compatible with an NLI-1/2 cask. The basket design also facilitated the postirradiation examination (PIE) fuel operations. The FRSB was loaded with the 12 removable fuel rods chosen for the PIE program during the Surry EOC-5 onsite examination and was stored in the spent fuel pool at the Surry site prior to shipment. A failed fuel can was used in this shipment to limit the potential for cask contamination.

After arrival of the shipping cask at the Surry site, the loading sequence consisted of the following steps:

(1) Lowering of the shipping cask into the spent fuel pool
(2) Inserting the FRSB into the failed fuel can
(3) Positioning the spacer assembly on top of the FRSB inside the failed fuel can
(4) Positioning the shipping cask lid
(5) Attaching the lifting rig
(6) Tightening the lid stud bolts
(7) Lifting of the shipping cask from the spent fuel pool
(8) Decontaminating the shipping cask
(9) Performing the pressure seal leak test
(10) Completing the cask surface activity survey

After successful completion of all of these steps, the shipping cask was loaded on the truck and secured for the trip to the BCL site. The truck left the Surry site on April 21, 1983.

The shipping cask was received at BCL's West Jefferson site on April 22, 1983. It was unloaded in accordance with the approved procedure. The FRSB was stored in the BCL storage pool until June 7, 1983, when it was transferred to the high energy cell. There the identification of the 12 rods was verified and they were individually transferred from the FRSB to a basket for storage in the high energy cell. The empty FRSB was returned to the storage pool.

# SECTION 4
# NONDESTRUCTIVE EXAMINATIONS

The following paragraphs discuss the results of the PIE on the selected 12 removable fuel rods. The work scope for both the nondestructive examinations and the destructive examinations is presented in table 4-1.

## 4-1. STEREOVISUAL EXAMINATION

A stereoscopic visual examination of all 12 fuel rods was performed to characterize their surface for distribution and nature of crud deposits, appearance of Zircaloy corrosion films, and incidences of unusual features, such as ridging, hydride blisters or fretting. The 12 rods were examined at 0- and 180-degree orientations using a Bausch and Lomb stereomacroscope at a magnification of approximately 3X. Photographs were taken at many of the axial positions where characterized pellets were located and metallographic examinations were planned. These pellets were located at approximately the 5-, 38-, 108-, and 130-inch elevations. Most of the photos were taken in the high-power region (30 to 130 inches) of the rods. However, other areas of the rod were photographed -- those where unusual crud and/or oxide patterns were observed.

The visual examination of the fuel rods was accomplished by holding the rods in a flat horizontal tray which moved in a horizontal plane beneath the objective lens of the variable-magnification stereo viewer. The axial field of view of a rod was approximately 1.0 to 1.5 inches long. A corresponding portion of an extended steel measuring tape was viewed simultaneously. The tape allowed the axial position of any visible feature on the rod surface to be identified.

The overall surface appearance of both the three- and four-cycle fuel rods was excellent. All the rods were essentially free of any tenacious crud or anomalous surface features. In general, the lower portions of the fuel rods (0 to 20-inch elevation) exhibited a very thin uniform black oxide layer, as depicted in figure 4-1. Further up the rods (near the 40-inch elevation), a

# TABLE 4-1

## HOT CELL WORK SCOPE

| Examination | Fuel Rod | | | | | | | | | | | |
|---|---|---|---|---|---|---|---|---|---|---|---|---|
| | 501 | 502 | 507[a] | 509 | 511 | 512 | 513 | 515[a] | 888(E9) | 888(M11) | 889(D7)[a] | 889(M9)[a] |
| Nondestructive | | | | | | | | | | | | |
| Visual examination | X | X | X | X | X | X | X | X | X | X | X | X |
| Profilometry | X | X | X | X | X | X | X | X | X | X | X | X |
| Gamma scan | X | X | X | X | X | X | X | X | X | X | X | X |
| Rod length | X | X | X | X | X | X | X | X | X | X | X | X |
| Eddy current oxide measurement | X | X | X | X | X | X | X | X | X | X | X | X |
| Destructive | | | | | | | | | | | | |
| Fission gas analysis | X | X | X | X | X | X | X | X | X | X | X | X |
| Void volume measurement | X | X | X | X | X | X | X | X | X | X | X | X |
| Clad/fuel metallography | | | X | | X | | X | | X | | | |
| Fuel density | | | X | | X | | X | | | | | |
| Burnup analysis | | | X | | X | | X | | | | | |
| MN-54 analysis | | | X | | X | | X | | | | | |
| $H_2$ analysis | | | X | | X | | X | | X | | | |

a. Three-cycle rods; the other eight are four-cycle rods.

white oxide corrosion layer was present, as shown in figure 4-2. This formation is typical of Zircaloy-4 rods when they have been irradiated for several cycles. The white oxide surface extended over the top third of the rods. Figure 4-3 shows the streaky white corrosion layer at the 110-inch elevation on Rod 512. Grid insertion scratches are also evident in the photograph. At slightly higher rod elevations, where the clad surface temperature is near its maximum, the white oxide layer generally appeared more patchy than at other regions, as shown in figure 4-4.

A number of the fuel rods also exhibited localized areas of spotty white oxide, as shown in figure 4-5. Grid locations were also examined for evidence of fretting or slippage. A grid contact mark is shown in figure 4-6. No significant wear was observed at any of the grid locations.

Six of the 12 rods examined (501, 502, 509, 511, 512, 515) had previously been brush cleaned during onsite inspections at the end of irradiation Cycle 2 and/or Cycle 4. The surface condition of these rods appears similar to those which were not cleaned. This indicates that very little crud was deposited on the rods during their irradiation in assembly RD-2. In addition, no difference in surface features was apparent between the three- and four-cycle rods or between the two four-cycle rods with different power histories.

## 4-2. FUEL ROD LENGTH MEASUREMENTS

In-cell length measurement of the rods was accomplished by comparing their length to that of a calibrated stainless steel standard. Each rod was placed against a stop, and a micrometer was adjusted to contact the top end plug. The micrometer reading was recorded, and the standard was then measured in the same manner. Each rod was measured along three orientations (0, 120, and 240 degrees) and the results were averaged. The temperatures of the fuel rod surface and the standard were recorded at the time of the measurements with a calibrated thermocouple. The rod length data were also corrected for thermal expansion.

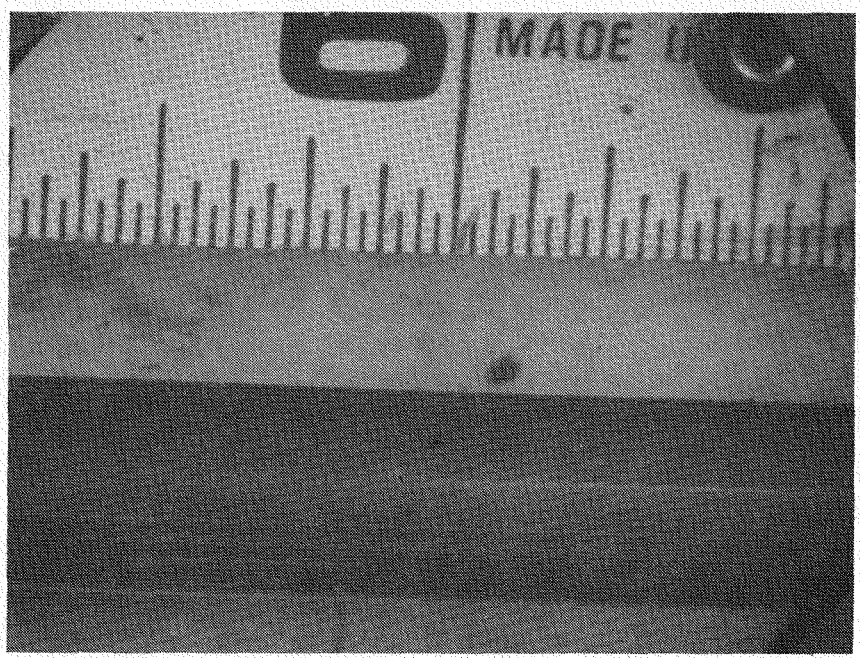


Figure 4-1. Typical Thin Black Oxide on Rod 511, 6-Inch Elevation, 0-Degree Orientation

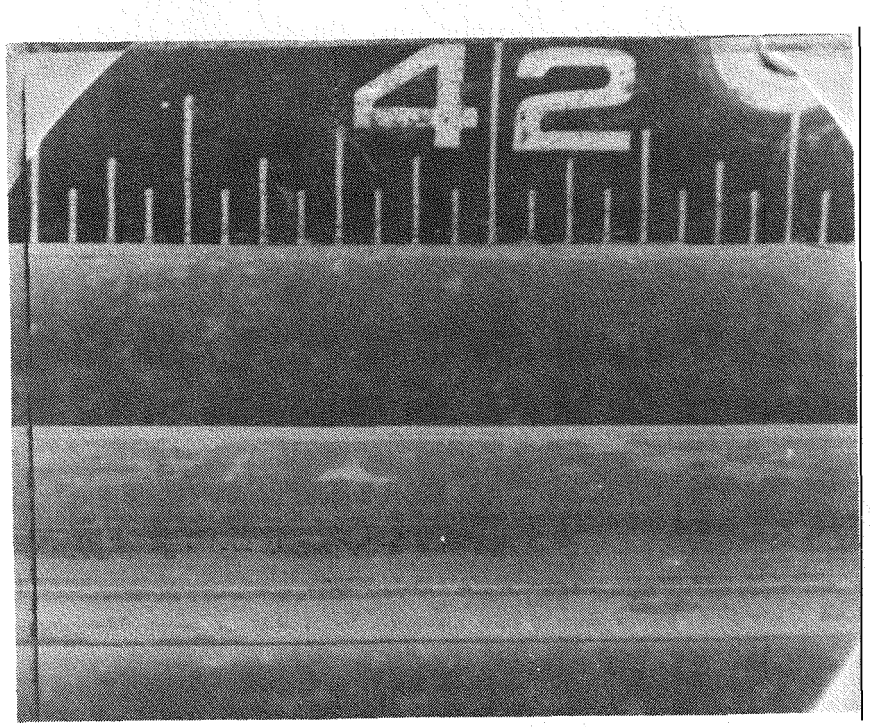


Figure 4-2. White Oxide Layer Present Over Many Areas of Surface on Rod 511, 42-Inch Elevation

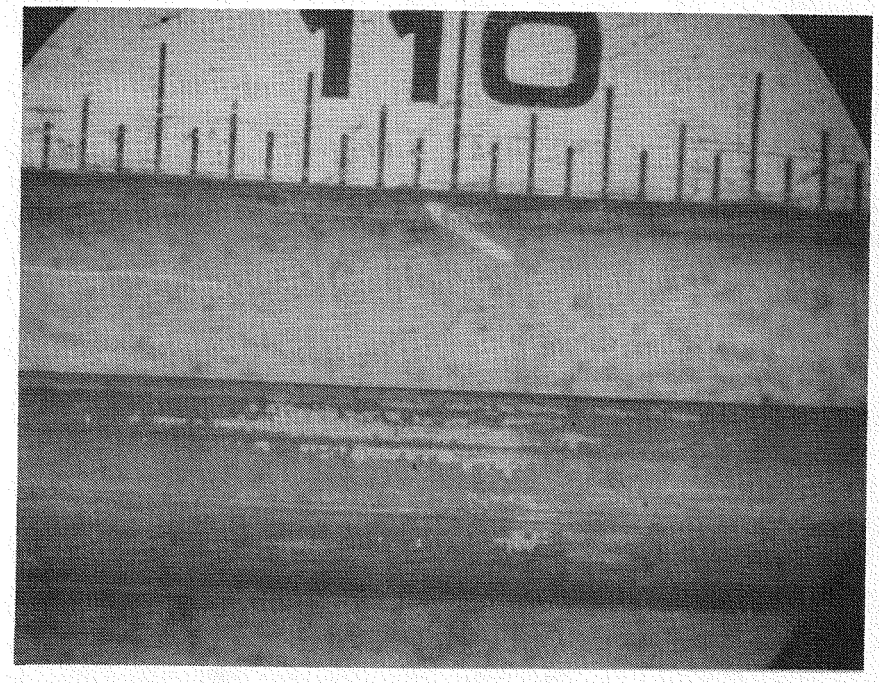


Figure 4-3. Typical Streaky White Oxide Found on Rod 512 at 110-Inch Elevation

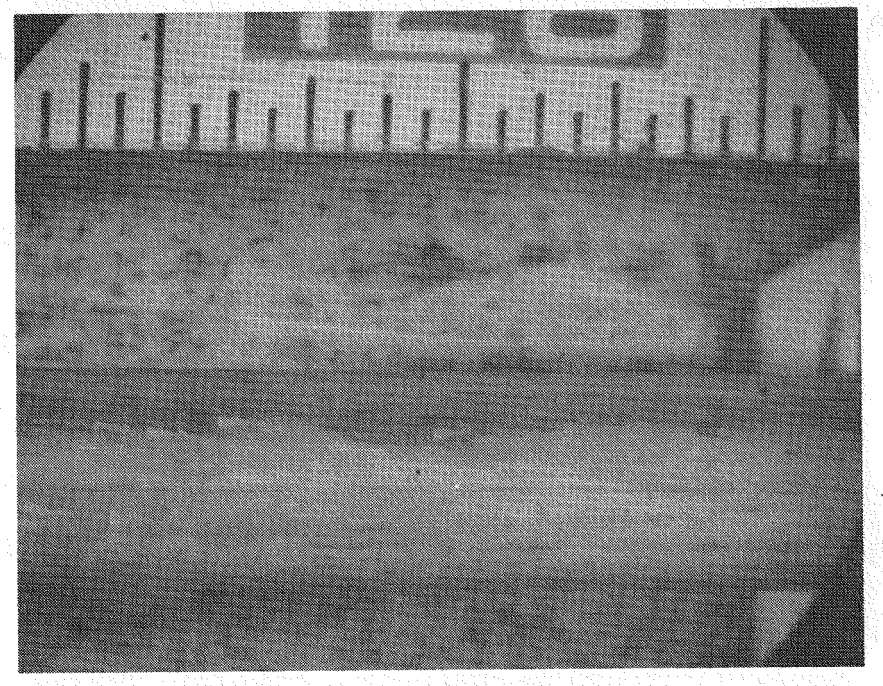

Figure 4-4. Thick White Patchy Oxide at 128-Inch Elevation of Rod 513

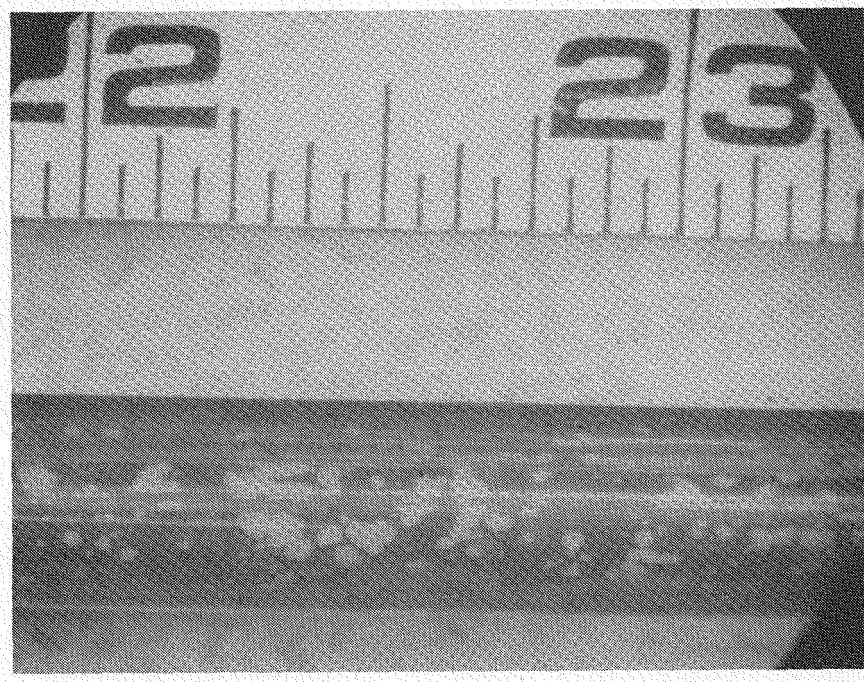


Figure 4-5. Localized White Oxide Spots on Rod 512 at 22.5-Inch Elevation

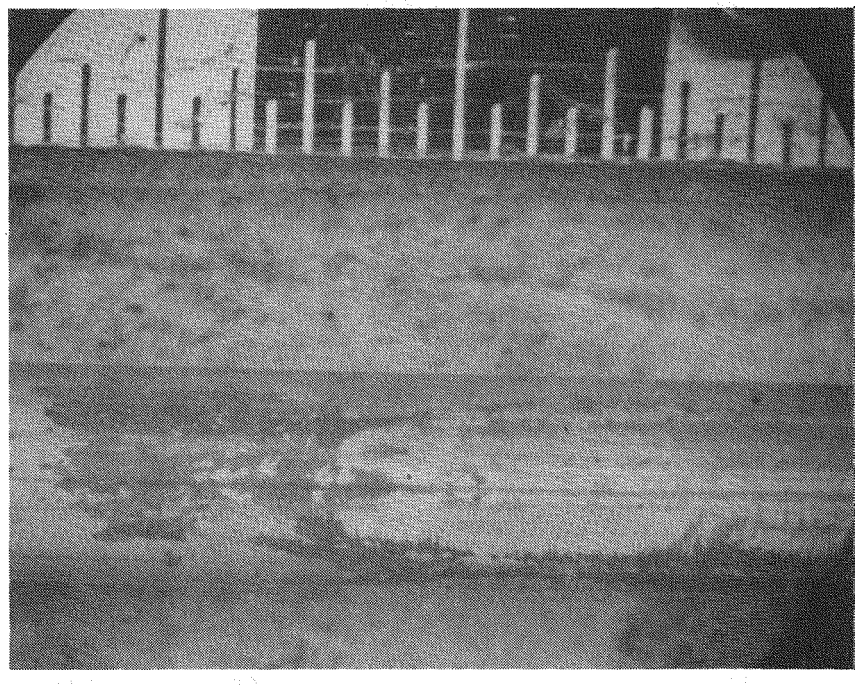

Figure 4-6. Grid Contact Mark on Rod 513, 131.8-Inch Elevation

The lengths of the rods were determined to an accuracy of 0.005 inch. The resultant data are presented in table 4-2. The length changes and percent rod growth for all 12 rods are shown in table 4-3. The four three-cycle rods exhibited an average length increase of 0.48 percent, and the eight four-cycle rods showed an average rod growth of 0.59 percent. A plot of the rod growth as a function of rod average fast fluence is shown in figure 4-7.

These rod growth values agree with the previously reported peripheral rod data.[3] These values are also consistent with BR-3[5] and Zorita[4] extended burnup fuel data. The rod length changes indicate that neither growth saturation nor increased rod growth rates occur with increased burnup.

## 4-3. GAMMA ACTIVITY SCANNING

The axial distribution of both gross and Cs-137 gamma activity was measured on all 12 removable rods. The gamma scanner consisted of a lithium-drifted germanium detector connected to amplifiers and an analyzer, along with a fuel rod holder, and a drive mechanism for translating the rod past the detector, and collimator. During scanning, the rod was first traversed past the collimator at a rate of 5 to 10 inches per minute, which enabled the maximum activity to be checked, and the collimator was adjusted. The rod was then gamma scanned in a single pass from top to bottom at a rate of 2 inches per minute. The rods were scanned for gross gamma activity ($E > 0.5$ MeV) and isotope Cs-137 (0.63-0.68 MeV).

From the resulting recordings, the fuel stack lengths and plenum lengths could be determined. Comparison of these results with preirradiation data permitted the calculation of changes in the stack and plenum dimensions. These are tabulated along with the fuel rod length results in table 4-4. The stack length changes are plotted as a function of burnup in figure 4-8.

In general, the gamma scans were normal, with no significant gaps or pellet fragmentation observed in the fuel column. The gross gamma activity scans, for both the three- and four-cycle rods, showed typical activity depressions

TABLE 4-2

ROD LENGTH MEASUREMENT DATA

| Rod No. | Micrometer Reading at Indicated Orientation (in.) | | | Mean Length (in.) | Clad Surface Temperature[a] (F°) |
|---|---|---|---|---|---|
| | 0° | 120° | 240° | | |
| Standard[b] | 0.015 | 0.015 | 0.015 | - | 86.5 |
| 888 (M-13) | 0.751 | 0.748 | 0.752 | 153.252 | 89 |
| 507 | 0.414 | 0.415 | 0.414 | 152.916 | 90 |
| 511 | 0.615 | 0.615 | 0.615 | 153.116 | 91 |
| 513 | 0.687 | 0.688 | 0.687 | 153.188 | 92 |
| 888 (E-9) | 0.819 | 0.819 | 0.818 | 153.320 | 88 |
| 515 | 0.648 | 0.648 | 0.647 | 153.149 | 91 |
| 502 | 0.823 | 0.823 | 0.823 | 153.324 | 92 |
| 512 | 0.801 | 0.801 | 0.800 | 153.302 | 91 |
| 501 | 0.717 | 0.718 | 0.716 | 153.218 | 92 |
| 889 (D-7) | 0.711 | 0.711 | 0.710 | 153.212 | 89 |
| 509 | 0.889 | 0.888 | 0.888 | 153.390 | 91 |
| 889 (M-9) | 0.631 | 0.631 | 0.631 | 153.132 | 90 |
| Standard | 0.015 | 0.015 | 0.015 | - | 86.5 |

a. Hot cell ambient temperature = 85°F

b. Length of calibrated standard rod = 152.4955 in. at 72°F

TABLE 4-3

REMOVABLE FUEL ROD LENGTH MEASUREMENT RESULTS

| Rod No. | Number of Cycles | Estimated Rod Average Burnup (MWD/MTU) | Length Change (in.) | Change, ΔL/L (%) |
|---|---|---|---|---|
| 501 | 4 | 44900 | 0.841 | 0.552 |
| 502 | 4 | 43800 | 0.958 | 0.629 |
| 507 | 3 | 29600 | 0.557 | 0.366 |
| 509 | 4 | 44500 | 1.031 | 0.677 |
| 511 | 4 | 44300 | 0.748 | 0.491 |
| 512 | 4 | 43900 | 0.940 | 0.617 |
| 513 | 4 | 43300 | 0.822 | 0.539 |
| 515 | 3 | 30000 | 0.775 | 0.509 |
| 888 (E9) | 4 | 39600 | 0.954 | 0.626 |
| 888 (M13) | 4 | 40000 | 0.886 | 0.581 |
| 889 (D7) | 3 | 28900 | 0.846 | 0.555 |
| 889 (M9) | 3 | 28700 | 0.766 | 0.503 |
| Three-cycle average: | | | 0.736 | 0.483 |
| Four-cycle average: | | | 0.898 | 0.589 |

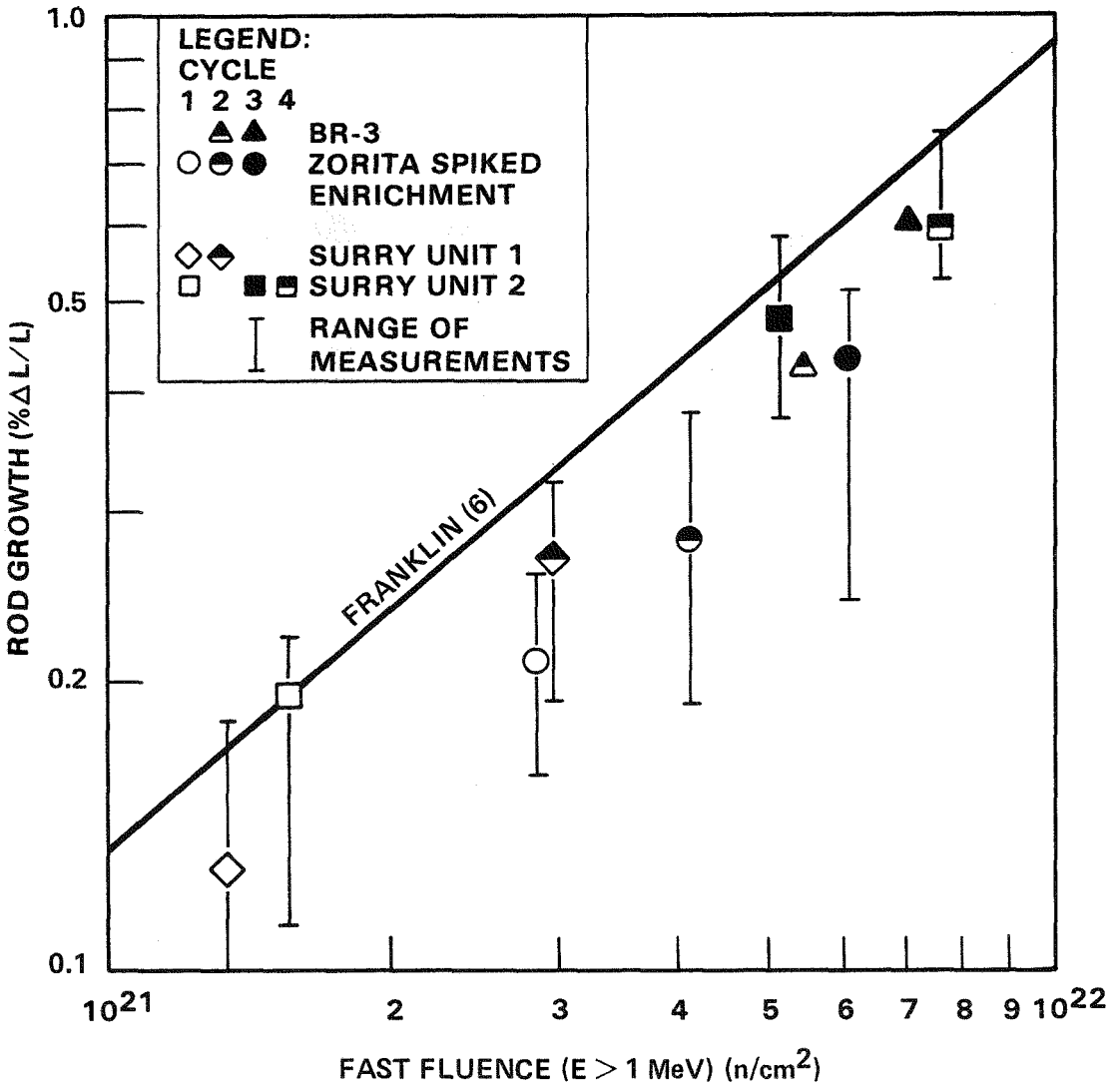


Figure 4-7. Surry Unit 2 Fuel Rod Growth as a Function of Rod Average Fast Fluence

# TABLE 4-4

## REMOVABLE FUEL ROD GAMMA SCAN MEASUREMENTS

| Rod No. | Plenum Length (in.) | | | Fuel Stack Length (in.) | | | Fuel Rod Length (in.) | | |
|---|---|---|---|---|---|---|---|---|---|
| | Before[a] | After[a] | Change | Before | After | Change | Before | After | Change |
| 501 | 6.18 | 6.328 | +0.148 | 144.121 | 144.814 | 0.693 | 152.377 | 153.218 | +0.841 |
| 502 | 6.14 | 6.185 | +0.045 | 144.150 | 145.063 | 0.913 | 152.366 | 153.324 | +0.958 |
| 507 | 6.23 | 6.276 | +0.046 | 144.052 | 144.563 | 0.511 | 152.358 | 152.915 | +0.577 |
| 509 | 6.12 | 6.313 | +0.193 | 144.162 | 145.000 | 0.838 | 152.358 | 153.389 | +1.031 |
| 511 | 6.07 | 6.102 | +0.032 | 144.222 | 144.938 | 0.716 | 152.368 | 153.116 | +0.748 |
| 512 | 6.22 | 6.350 | +0.130 | 144.065 | 144.875 | 0.810 | 152.361 | 153.301 | +0.940 |
| 513 | 6.15 | 6.362 | +0.212 | 144.140 | 144.750 | 0.610 | 152.366 | 153.188 | +0.822 |
| 515 | 6.10 | 6.447 | +0.347 | 144.197 | 144.625 | 0.428 | 152.373 | 153.148 | +0.775 |
| 888 (E9) | 6.15 | 6.619 | +0.469 | 144.140 | 144.625 | 0.485 | 152.366 | 153.320 | +0.954 |
| 888 (M13) | 6.15 | 6.308 | +0.158 | 144.140 | 144.868 | 0.728 | 152.366 | 153.252 | +0.886 |
| 889 (D7) | 6.15 | 6.636 | +0.486 | 144.140 | 144.500 | 0.360 | 152.366 | 153.212 | +0.846 |
| 889 (M9) | 6.15 | 6.556 | +0.406 | 144.140 | 144.500 | 0.360 | 152.366 | 153.132 | +0.766 |

a. Before (after) irradiation

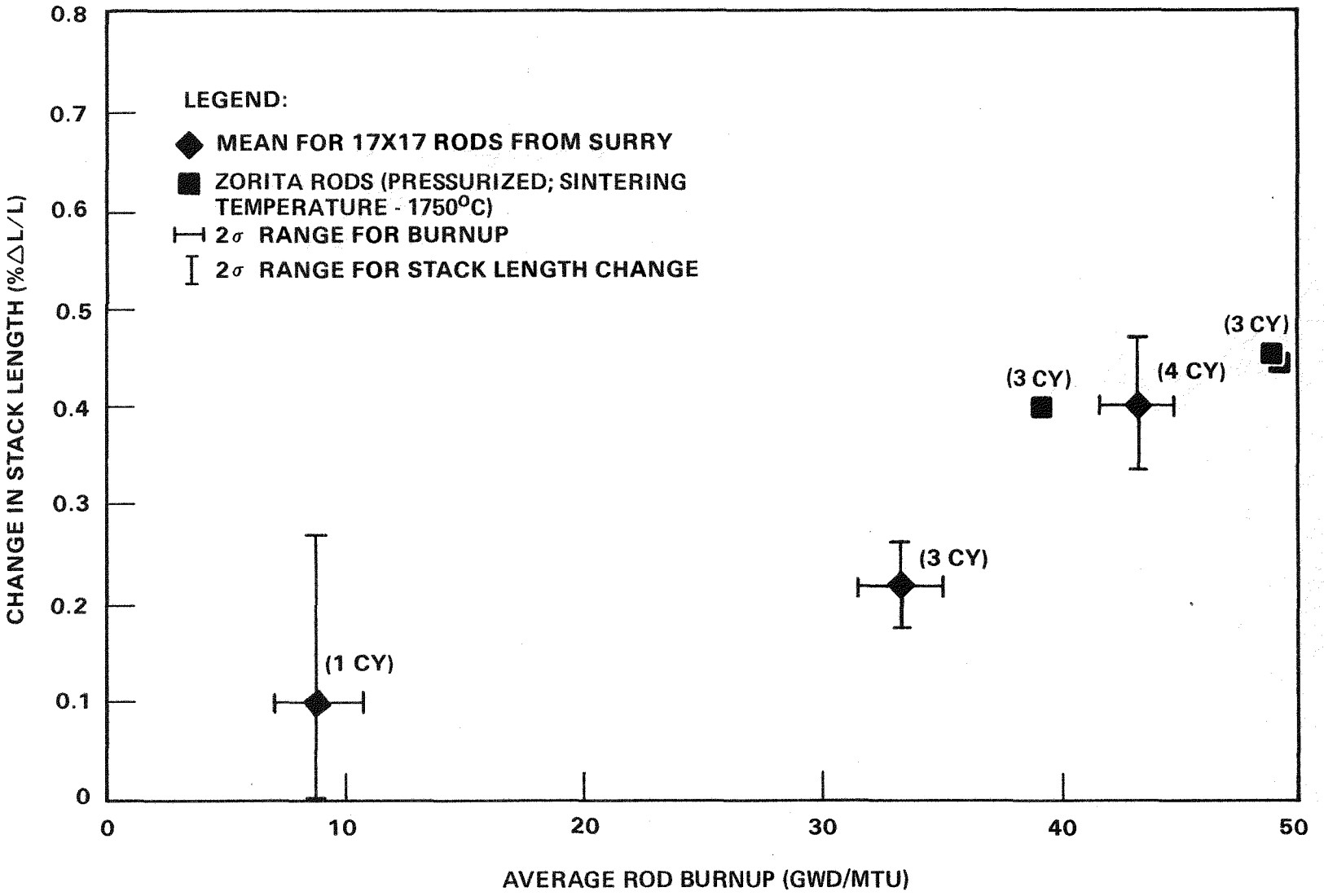


Figure 4-8. Surry Unit 2 Removable Rod Fuel Stack Length Changes With Burnup

at the pellet interfaces. This is clearly depicted in figure 4-9, which shows a portion of a gamma scan trace for fuel rod 511. A slight activity depression was also observed near the grid locations for all the rods. The Cs-137 gamma scans, an example of which is shown in figure 4-9, did not consistently exhibit repetitive sharp depressions at the pellet intervals. This indicates some migration of the volatile cesium. Both gamma scans provide a good indication of the burnup distribution within the fuel assembly.

The fuel stack length changes for the three- and four-cycle fuel rods, as shown in figure 4-8, are consistent with increases seen with fuel at Zorita. The fuel column average growth was approximately 0.21 percent Δ for three irradiation cycles and approximately 0.40 percent Δ for four cycles. These fuel length increases are expected because of the stable fuel (approximately 1740°C sintering temperature) used in the Surry rods. This fuel shows good low burnup stability (minimal densification) and net fuel stack growth (because of the combined effects of fuel pore removal and swelling) at high burnups. If isotropic swelling and densification is assumed, then the four-cycle stack growth data (slope of best-estimate plot) produce an estimated net swelling rate of about 0.29 percent per 10,000 MWD/MTU. This fairly low swelling rate is in good agreement with the fuel pycnometric density data presented in section 5. In relation to the fuel rod growth, the fuel stack increases were much smaller for both the three- and four-cycle rods; this suggests a minimal amount of fuel-cladding mechanical interaction.

## 4-4. CLAD CORROSION MEASUREMENT

The thickness of oxide on the clad exterior of the Surry fuel rods was measured using an eddy current technique; the equipment consisted of a commercially available eddy current probe, an analog meter display (Permascope), and a strip chart recorder. A mechanical probe holder was used to position the probe perpendicular to the fuel rod to be measured.

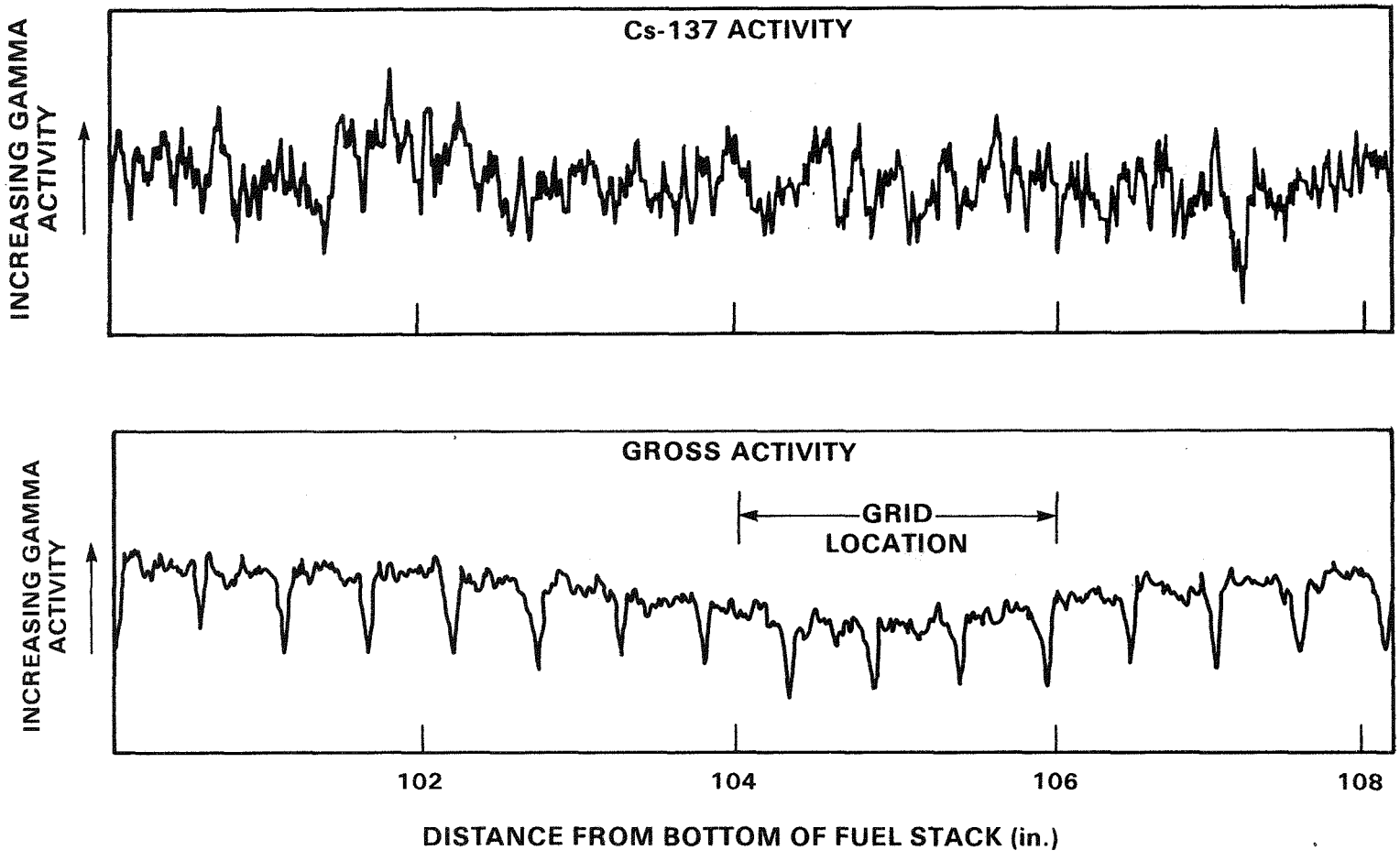


Figure 4-9. Sections of Gross and Cs-137 Gamma Activity Chart From High-Power Region of Rod 511

Before measurements were made on the fuel rods, the system was checked for normal and thermal drifts and for accuracy and precision using air-oxidized Zircaloy-4 tubes with known oxide film thicknesses. The maximum system deviation was $\pm$ 3 percent. The probe and the Permascope were calibrated against the tube standards for measurements made repeatedly at one location. All readings were found to be within a $\pm$ 2 μm range of the oxide thicknesses of the standards.

Hot cell measurement on the fuel rods was carried out by positioning the rod in the holding bed after brush crud removal. The probe was allowed to contact the fuel rod with a constant pressure of approximately 110 $g/mm^2$. A motor drive was used to move the probe at a constant speed (12 inches per minute) along a working length (35 inches) of the rod, thereby producing a continuous trace of the oxide thickness over the working length for a particular azimuthal orientation. This procedure was repeated until the entire length of the fuel rod had been scanned at specified orientations (0, 90, 180, and 270 degrees). Measurement on each fuel rod was preceded by a calibration check using the Zircaloy-4 tube standards. At the end of each fuel rod scan, the tube standard was remeasured to verify the accuracy of the system. A schematic diagram of the instrument is shown in figure 4-10.

Data were extracted from the continuous strip charts at 52 axial positions; the readings were averaged over $\pm$ 0.3 cm of the position, ignoring occasional sharp "blips" that could be attributed to foreign material on the rod surface. A typical section of an eddy current scan is shown in figure 4-11.

The eddy current trace (ECT) data were compared with corresponding Surry water-side corrosion measurements from metallography of clad outer diameters (section 5). The resultant plot of the data indicated slightly higher values for the eddy current measurements. Consequently, the eddy current values were corrected by obtaining a functional relationship between the ECT and metallographic data by linear regression analysis, as presented in appendix C, figure C-1. A correlation coefficient of 0.942 clearly indicated a strong linear relationship. Tables C-1 through C-12 in appendix C summarize the oxide measurements at selected axial positions for four individual orientations.

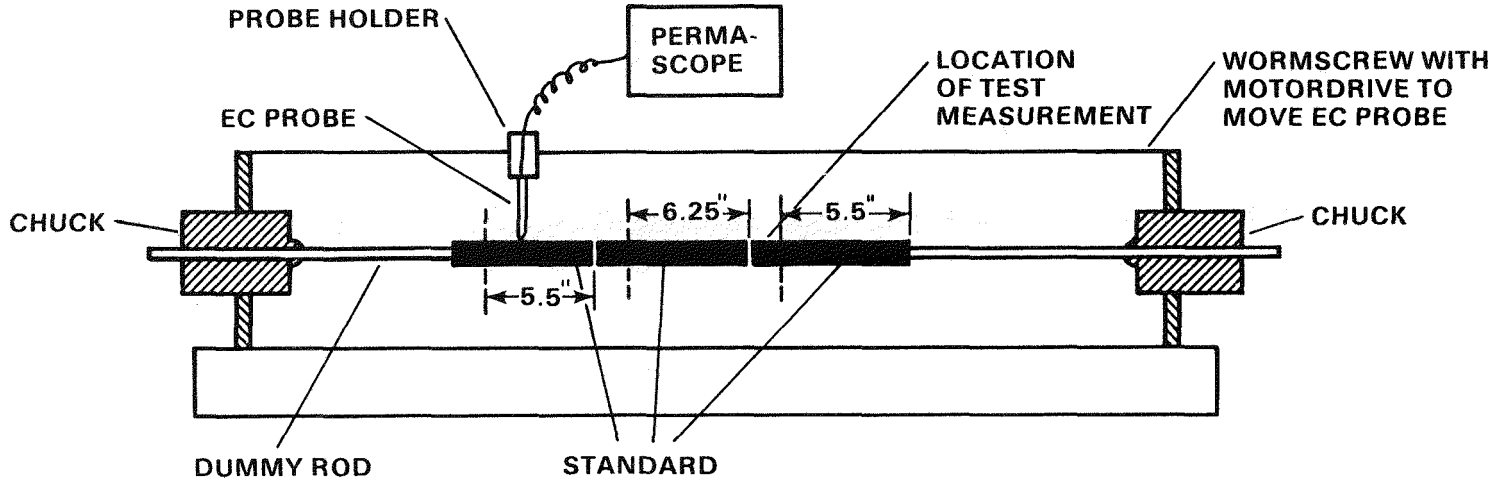


Figure 4-10. Schematic Diagram of Oxide Meter Instrument Arrangement

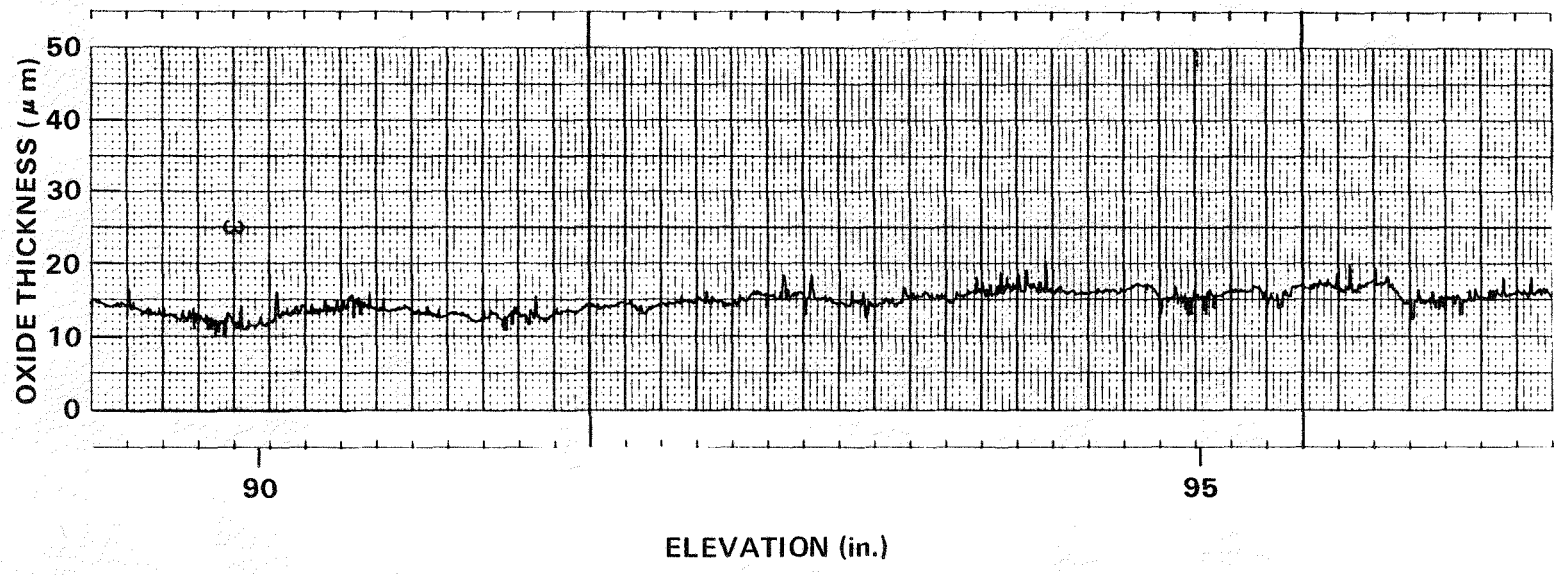


Figure 4-11. Typical Eddy Current Trace Showing Oxide Film Thickness on Rod 507, 0-Degree Scan

The eddy current traces exhibited similar trends for both the three- and four-cycle rods. As illustrated in figure 4-12, a gradual increase in the oxide thickness was evident from the rod bottom to the top. Oxide film thicknesses of approximately 0.2 to 0.3 mils at the bottom of both three- and four-cycle rods gradually increased up to about 0.5 mils and about 1.0 to 1.1 mils at the high surface temperature region (100 to 130 inches) of the rod for three- and four-cycle rods, respectively. These observations, which are typical of normal fuel rod power histories, can be attributed largely to the higher clad temperatures at the top of the rods resulting from the coolant temperature rise.

The eddy current traces also revealed a distinct decrease in oxide thickness at the grid locations, as shown in figure 4-12. This observation can be attributed to the power depression, increased flow turbulence, and local surface heat transfer coefficients downstream from the grid. A slight decrease in corrosion film thickness was also evident at the top of the fuel column (about 135.0 inches) for both three- and four-cycle rods -- again, a lower power region. Two four-cycle rods, which had initially been irradiated at slightly higher powers in assembly RD-1 for its first two cycles, had slightly higher peak corrosion values (1.2 mils versus 1.0 mils) than the other four-cycle rods.

## 4-5. FUEL ROD PROFILOMETRY

Profilometer traces were run on 12 fuel rods for diametral measurements and detection/characterization of local clad anomalies such as blisters, depressions, ridging and ovality.

### 4-5-1. Clad Diameter Measurements

Helical diametral scans were made on the four three- and eight four-cycle fuel rods, encompassing the fuel column and plenum regions between the upper and

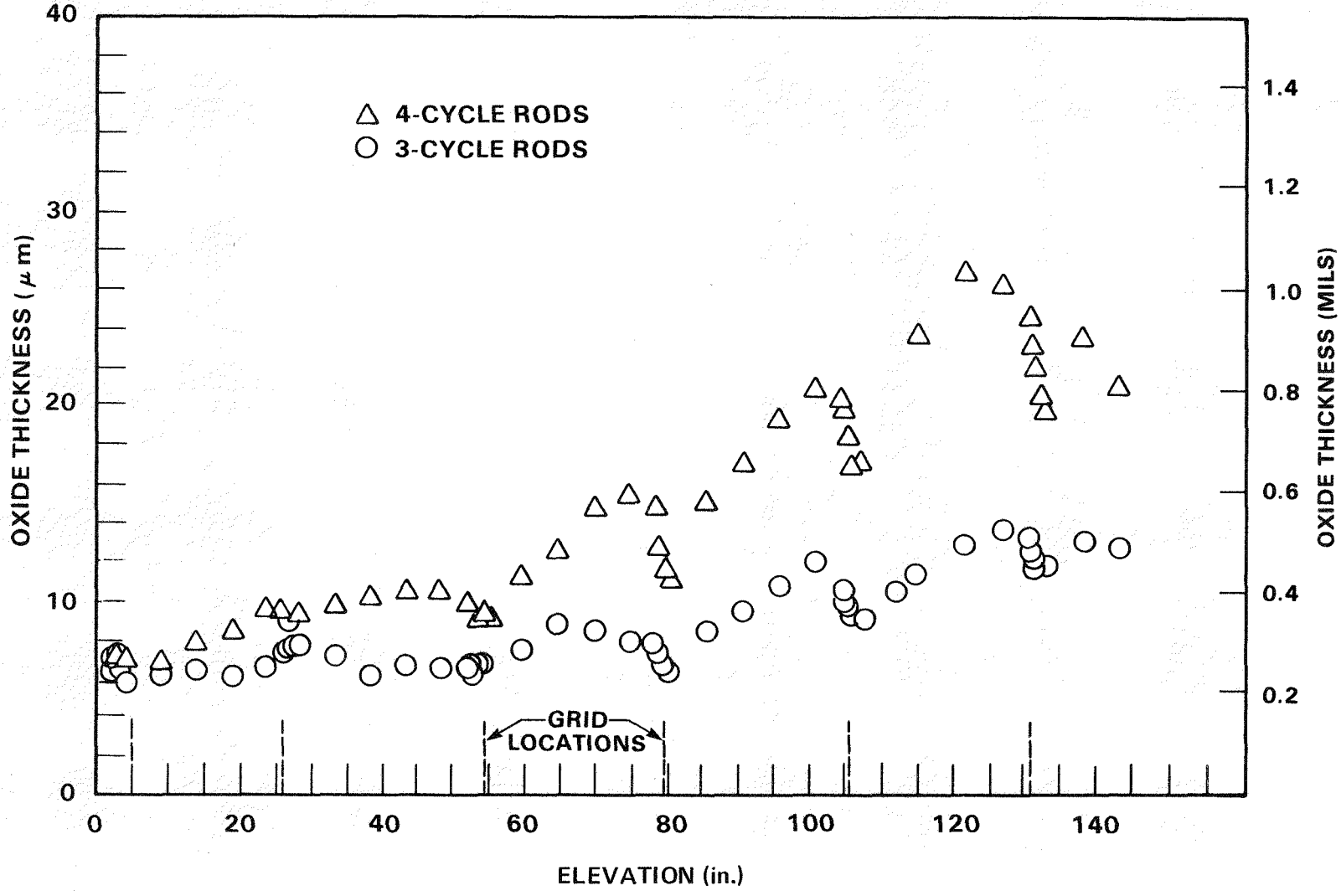


Figure 4-12. Average Corrosion Film Thickness on Surry Unit 2 Fuel Rods (Bias-Corrected Data)

lower end plug weld zones. A pitch of 0.100 inch was used as the rods were translated past the transducer head by means of a precision lathe screw drive; the ends of the rods were held in rotating chucks. All the rods were wiped clean with a cloth prior to profilometry. A step standard of diameters above and below the fuel rod nominal diameter was run for calibration. Each rod was marked at 35-, 70-, 105-, and 140-inch elevations. The rods were then loaded into the profilometer and scanned in 35-inch segments from bottom to top at 2 inches per minute axial travel of the sensing heads. The step standard was run after each rod profile to assure measurement quality. The measured precision of the system was $\pm$ 0.2 mil (2 $\sigma$) on clad diameter and $\pm$ 0.8 mil (2 $\sigma$) on length positioning.

Average clad diameter values were reduced from the strip charts at 13 elevations; the data for each rod are tabulated in appendix D, tables D-1 through D-6. The data at each position represent an average value of seven measurements taken within the interval $\pm$ 0.75 inch of the exact location.

Clad ovality (maximum diameter minus minimum diameter) at each position is also listed. The preirradiation diameters (from micrometer measurements) are tabulated, as well as the diameter changes, $\Delta D$, in mils.

Five of the eight four-cycle fuel rods that were examined had previously been profiled after one and three irradiation cycles; they continued to exhibit creepdown at every elevation. Data from the other three four-cycle rods were consistent with the same basic trend. Figure 4-13 shows the extent of creepdown of the rods for one, three, and four cycles of irradiation. A typical axial profile of clad diameter changes was exhibited for all of the rods, with a diameter minimum at the 25- to 50-inch zone, the highest power region of the rods, and diameters approaching the preirradiation values at the extremes of the rods. The rod average clad creepdown for the individual rods is tabulated in table 4-5. The maximum average creepdown for the characterized four-cycle rods was 2.7 mils. The incremental average creepdown from three to four cycles was 0.32 mil, a much smaller step change than for the previous cycles.

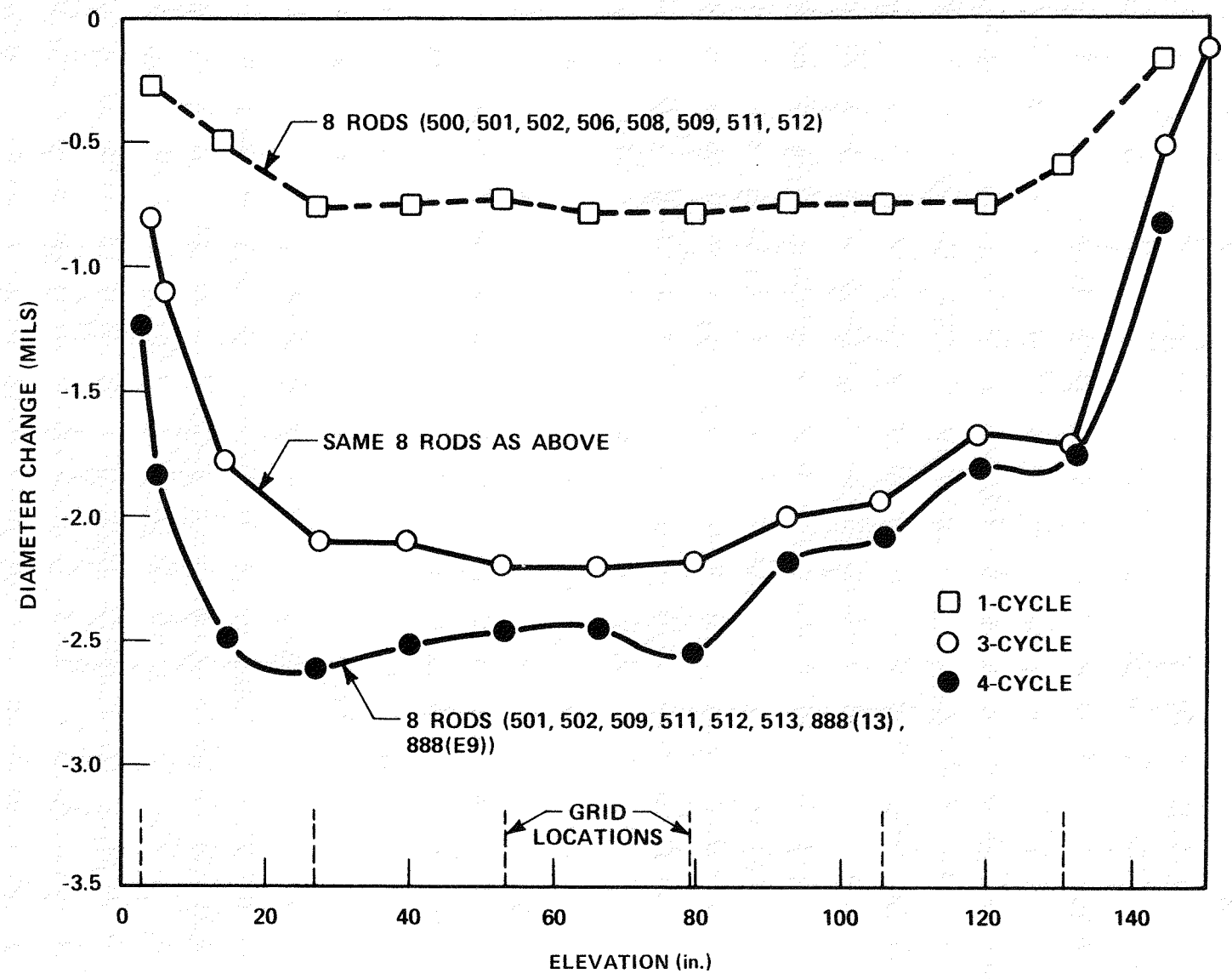


Figure 4-13. Average Clad Creepdown of Surry Unit 2 Fuel Rods

TABLE 4-5

SUMMARY OF AVERAGE CLAD CREEPDOWN DATA FROM

THREE- AND FOUR-CYCLE REMOVABLE RODS

| Rod No. | Number of Cycles | Average Burnup (MWD/MTU) | Average Power Level (kw/ft) | Diametral Creepdown[a] at Indicated Cycle (mils) | | | |
|---|---|---|---|---|---|---|---|
| | | | | 1-Cycle | 2-Cycle | 3-Cycle | 4-Cycle |
| 507 | 3 | 29570 | 4.95-5.52 | -- | -- | 2.3 | -- |
| 515 | 3 | 29980 | 5.13-5.62 | 0.8 | -- | 2.6 | -- |
| 501 | 4 | 44900 | 5.09 | 0.6 | -- | 2.0 | 2.2 |
| 502 | 4 | 43800 | 5.01 | 0.9 | -- | 2.1 | 2.4 |
| 509 | 4 | 44500 | 4.97 | 1.0 | -- | 2.4 | 2.4 |
| 511 | 4 | 44300 | 4.99 | 0.6 | -- | 1.8 | 2.1 |
| 512 | 4 | 43900 | 5.05 | 0.4 | -- | 1.4 | 2.2 |
| 513 | 4 | 43300 | 4.91 | -- | -- | -- | 2.7 |

CYCLE-WISE INCREMENTAL CREEPDOWN[a]

| Cycle | 1 | 2 | 3 | 4 |
|---|---|---|---|---|
| EFPH | 6320 | 6620 | 9670 | 9840 |
| ΔD (mils) | 0.72 | NA | 0.64 | 0.32 |
| Number of rods | 8 | -- | 7 | 6 |

a. Over high-power region of fuel, 27.0-to 118.7-inch elevations

## 4-5-2. Characterization of Rod Surface Variations

The overall surface condition of the three- and four-cycle fuel rods, as indicated by the profilometry traces, was good. The major features found were isolated cases of high ovality and ridging on some of the rods, with almost no incidences of significant depression. There were also no indications of significant clad anomalies, such as clad blisters or fretting.

Average clad ovality, as compiled for the individual fuel rods in table 4-6, ranged between 0.7 and 1.4 mils for the four-cycle rods. Changes in ovality from the three-cycle data were small. In fact, very little change in ovality was seen in the fuel rods after the first irradiation cycle. An example of localized cases of high ovality, along with fairly high ridging, is shown in figure 4-14. Rod 509 exhibited ovalities greater than 4.0 mils at the 126.5- and 129.0-inch elevations.

TABLE 4-6

SUMMARY OF THREE- AND FOUR-CYCLE REMOVABLE ROD CLAD OVALITY CHANGES

| Rod | Number of Cycles | Average Clad Ovality at Indicated Cycle[a] (mils) | | | | |
|---|---|---|---|---|---|---|
| | | Preirradiation | 1 Cycle | 2 Cycles | 3 Cycles | 4 Cycles |
| 507 | 3 | 0.1 | -- | -- | 1.9 | -- |
| 515 | 3 | 0.1 | 2.0 | -- | 1.3 | -- |
| 501 | 4 | 0.2 | 1.7 | -- | 1.3 | 0.9 |
| 502 | 4 | 0.3 | 1.4 | -- | 1.1 | 1.1 |
| 509 | 4 | 0.4 | 1.6 | -- | 1.9 | 1.1 |
| 511 | 4 | 0.2 | 1.6 | -- | 1.4 | 1.4 |
| 512 | 4 | 0.3 | 1.0 | -- | 1.3 | 1.2 |
| 513 | 4 | 0.1 | -- | -- | -- | 0.65 |
| Average of two three-cycle rods | | -- | 1.0 -- | -- | 1.6 | -- |
| Average of six four-cycle rods | | -- | 1.5 -- | -- | 1.4 | 1.4 |

a. Over high-power region of fuel, 27.0-to 118.7-inch elevations

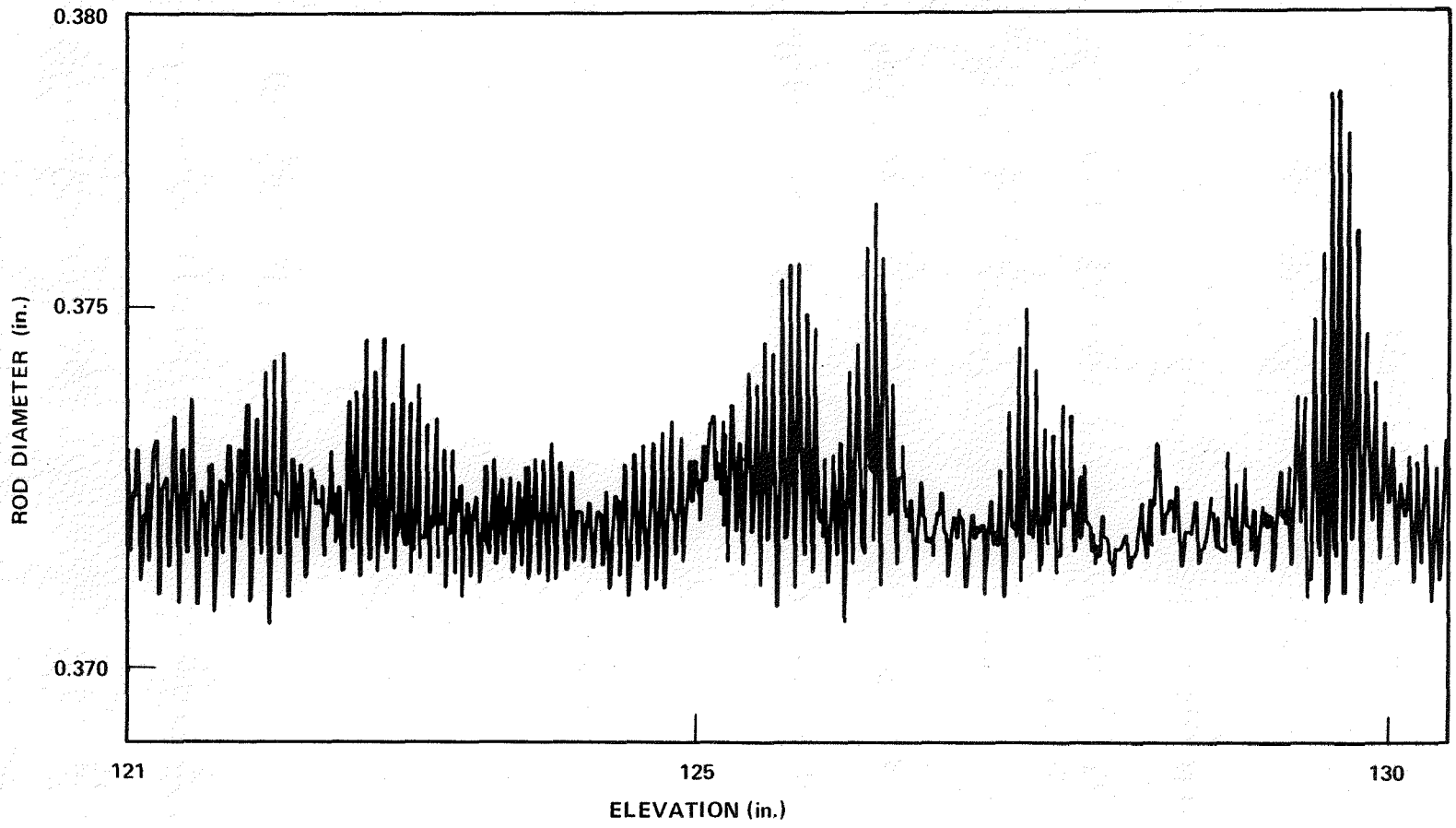


Figure 4-14. Typical Profilometry Trace of Rod 509 Showing Incidences of Ridging and Ovality

# SECTION 5
# DESTRUCTIVE EXAMINATIONS

## 5-1. FISSION GAS ANALYSIS AND INTERNAL VOID VOLUME MEASUREMENT

All 12 fuel rods were punctured to collect fission gas and to measure the internal void volume. The gas release was calculated by comparing the moles of fission gas collected, as determined by mass spectrometry and gas inventory, to the total number of moles of gas generated, using rod average burnup values developed from the rod power history data. The calculated fission gas release values are listed in table 5-1; the internal void volumes for the same 12 rods are tabulated in table 5-2. The elemental and isotopic fission gas analyses are given in appendix E.

The Surry fuel rods, as shown in table 5-1, had consistently low gas releases (less than 0.6 percent). The three- and four-cycle rods had average gas releases of 0.3 and 0.5 percent, respectively. The results showed very little scatter in the fission gas released within the two burnup groups ($\sigma$ = 0.05 percent at 30 GWD/MTU and 0.04 percent at 40-45 GWD/MTU). The data indicate a very slight burnup dependency on gas release.

The low gas release values were not unexpected, considering the low power levels (4 to 5 kw/ft) at which the rods operated. Figure 5-1 presents the fission gas release data as a function of burnup for a number of high- and low-powered rods from different reactors. The Surry data were very consistent with those from all other low-powered rods. In contrast, the high-powered rods (more than 10 kw/ft) from Zorita and BR-3[4,5] displayed significant gas release (4 to 36 percent) and a very strong dependency on fuel temperature.

The low fission gas release was also expected, based on the Surry fuel microstructure (paragraph 5-2-1). There was no indication of any gas bubble formation along the grain boundaries or extensive grain growth at the fuel center that is seen in fuel with high levels of gas release. The fuel structure was very typical of low-powered fuel that had been irradiated at low temperatures and released only a very small amount of fission gas.

TABLE 5-1

FISSION GAS RELEASE RESULTS

| Rod No. | Average Burnup (MWD/MTU) | Total Gas Collected ($cm^3$ at STP) | Xe + Kr[a] Collected ($cm^3$ at STP) | Xe + Kr Produced ($cm^3$ at STP) | Measured[b] Gas Release (%) |
|---|---|---|---|---|---|
| 501 | 44900 | 587.49 | 13.69 | 2344 | 0.58 |
| 502 | 43800 | 563.01 | 11.71 | 2291 | 0.51 |
| 507 | 29600 | 553.65 | 3.71 | 1543 | 0.24 |
| 509 | 44500 | 579.17 | 13.09 | 2327 | 0.56 |
| 511 | 44300 | 570.62 | 12.61 | 2315 | 0.54 |
| 512 | 43900 | 580.58 | 12.31 | 2293 | 0.54 |
| 513 | 43300 | 566.31 | 10.25 | 2259 | 0.45 |
| 515 | 30000 | 585.11 | 3.57 | 1564 | 0.23 |
| 888 (E9) | 39600 | 602.47 | 11.87 | 2065 | 0.57 |
| 888 (M13) | 40000 | 608.21 | 12.53 | 2087 | 0.60 |
| 889 (D7) | 28900 | 591.37 | 5.20 | 1506 | 0.34 |
| 889 (M9) | 28700 | 591.12 | 4.37 | 1495 | 0.29 |

a. As determined from mass spectroscopy analysis

b. Based on 200 MeV/fission and 0.3 atoms Xe + Kr per fission

TABLE 5-2

FISSION GAS DATA AND INTERNAL VOID VOLUMES

| Rod No. | Burnup (MWD/MTU) | Total Gas Collected ($cm^3$ at STP) | Internal Void Volume ($cm^3$) |
|---|---|---|---|
| 888 (E9) | 39600 | 602.47 | 15.41 |
| 507 | 29600 | 553.65 | 15.36 |
| 511 | 44300 | 570.62 | 13.85 |
| 513 | 43300 | 566.31 | 14.74 |
| 888 (M13) | 40000 | 608.21 | 14.44 |
| 515 | 30000 | 585.11 | 16.00 |
| 502 | 43800 | 563.01 | 14.26 |
| 512 | 43900 | 580.58 | 14.88 |
| 501 | 44900 | 587.49 | 14.72 |
| 509 | 44500 | 579.17 | 14.68 |
| 889 (M9) | 28700 | 591.12 | 15.93 |
| 889 (D7) | 28900 | 591.37 | 14.99 |

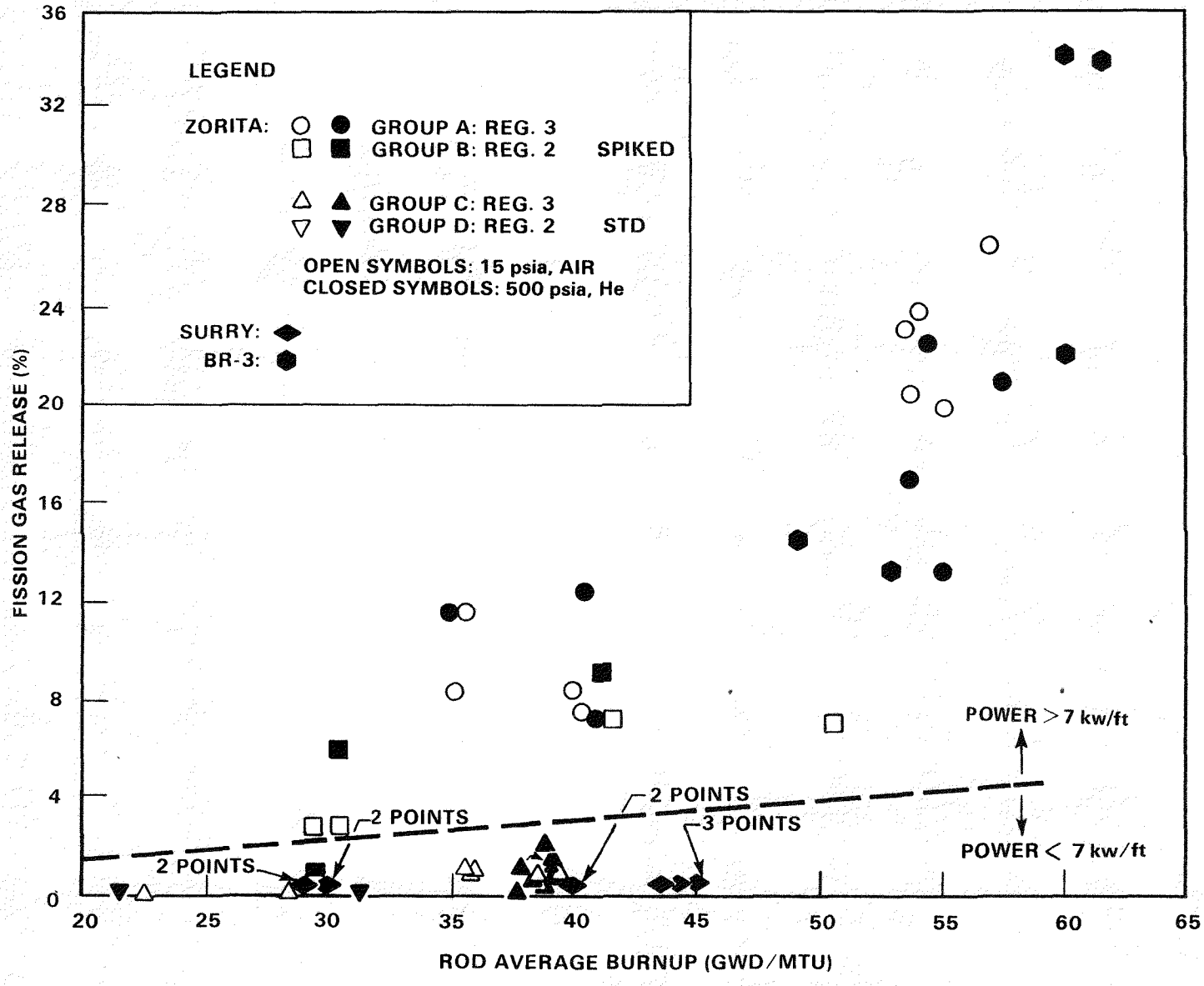


Figure 5-1. Surry Unit 2 Fission Gas Data Compared With Data From Other Plants

The initial helium gas inventory of the fuel rods, based upon nominal preirradiation rod dimensions, should have been approximately 524 $cm^3$ at standard temperature and pressure (see appendix F). All the rods yielded amounts of helium consistent with this estimate (within analytical error); the data therefore give confidence that all the internal gases were collected. The measured internal void volume of the fuel rods, as listed in table 5-2, averaged between 13.85 and 16.00 $cm^3$ and was not significantly affected by rod burnup or enrichment.

## 5-2. CLADDING AND FUEL METALLOGRAPHY

### 5-2-1. Water-Side Corrosion/Hydriding

Nine sections from four fuel rods were examined metallographically for water-side corrosion. Appendix G outlines the specific metallographic section locations on the fuel rods. Each clad/fuel metallographic sample was prepared by cutting a 1-inch section from the rod, vacuum impregnating it with epoxy, and then making a secondary cut through the sample at the intended plane of examination. The transverse fuel/clad sections were mounted within stainless steel guard rings to minimize clad edge rounding during sample preparation. Each transverse metallographic sample also included an orientation index marker, corresponding to 0 degrees and referencing the center digit of the stamped rod number on the cladding. Photographs were taken of the exterior oxide layer, and the etched cladding was examined for hydrogen precipitates at four orientations (0, 90, 180, and 270 degrees).

Table 5-3 summarizes the circumferential average water-side corrosion measured at selected axial positions along the four fuel rods. Samples were selected from high (38- to 109-inch) power regions and also moderate (130- to 135-inch) and low (5.5-inch) power zones. As expected, the average water-side oxide corrosion thickness was greatest near the top of the fuel rods (at about 133 inches). This can be attributed largely to the higher clad temperatures at these locations as a result of the bulk coolant temperature rise. The least amount of oxidation was observed near the bottom of the rods (at about 5.5 inches).

TABLE 5-3

METALLOGRAPHIC WATER-SIDE CORROSION THICKNESS MEASUREMENTS

| Rod No. | Elevation (in.) | Local Burnup (GWD/MTU) | Average Oxide Thickness at Indicated Orientation (mils) | | | | |
|---|---|---|---|---|---|---|---|
| | | | 0° | 90° | 180° | 270° | Overall |
| 507 | 108.5 | 30.4 | 0.25 | 0.25 | 0.22 | 0.19 | 0.23 |
| | 135.5 | 20.4 | 0.28 | 0.44 | 0.25 | 0.34 | 0.33 |
| 511 | 5.5 | 31.9 | 0.09 | 0.09 | 0.09 | 0.11 | 0.10 |
| | 38.5 | 48.3 | 0.19 | 0.25 | 0.25 | 0.11 | 0.20 |
| | 133.5 | 39.4 | 0.50 | 0.66 | 0.50 | 0.59 | 0.56 |
| 513 | 103.8 | 46.3 | 0.50 | 0.56 | 0.52 | 0.56 | 0.54 |
| | 108.7 | 46.3 | 0.47 | 0.44 | 0.50 | 0.52 | 0.48 |
| 888 (E9) | 130.0 | 37.6 | 1.0 | 1.0 | 0.86 | 1.0 | 0.97 |
| | 133.6 | 35.2 | 0.75 | 0.72 | 0.62 | 0.66 | 0.69 |

The peak water-side corrosion of the rods (as obtained from the corrected oxide meter measurements) has been plotted as a function of peak rod burnup in figure 5-2. Selected data from other plants[4,5] are also illustrated. It is to be noted that, although the absolute level of corrosion is low, the Surry data showed a two-fold increase in corrosion film thickness between three and four cycles of irradiation (29,690 to 42,970 MWD/MTU). The peak water-side corrosion after three cycles of irradiation was 0.42 mils, while for six of the eight four-cycle rods, all of which had the same relative power rating in assembly RD-2, a peak circumferential average corrosion of 0.85 mils was observed. The other two four-cycle rods, which had initially been irradiated at higher power levels in assembly RD-1 for their first two cycles, exhibited a slightly higher peak corrosion, 1.10 mils. However, these two rods of lower enrichment operated at lower power and achieved lower accumulated burnup during the last two cycles of operation. The magnitude of water-side corrosion in the Surry rods is slightly greater than that observed for BR-3 and Zorita rods and is attributed to slightly higher coolant temperatures.

Figures 5-3 and 5-4 show the typical appearance of the clad exterior corrosion layer of both three- and four-cycle fuel rods at the same high-power axial position. A section of the cladding that had been etched for hydrogen precipitates is also shown. The exterior corrosion films were generally uniform in thickness at all four orientations. Although there was little or no indication of any radial cracks through the oxide, there were areas where an upper section of the layer had broken away or had flaked off. No evidence of any crud could be detected on the corrosion film surface. An obvious increase in the oxide thickness was apparent from the three- to the four-cycle rod, as shown in figures 5-3 and 5-4. An example of the maximum corrosion layer (approximately 1 mil) found in the four-cycle rods is presented in figure 5-5.

The hydrogen precipitates depicted in figures 5-3 through 5-5 generally are short and circumferentially oriented after three cycles and markedly longer and thicker after four cycles. This observation is quite consistent with the hydrogen analyses discussed in paragraph 5-3.

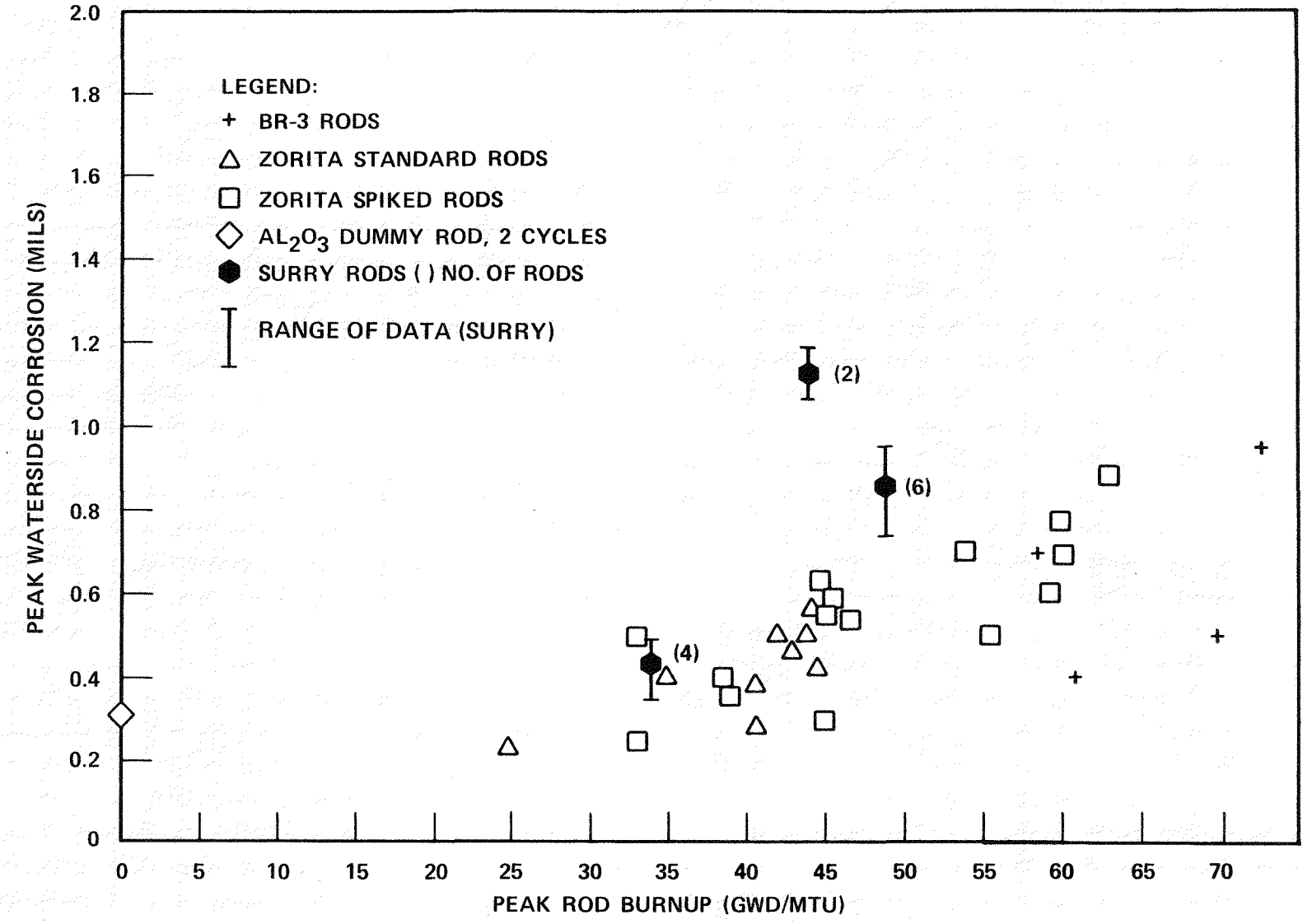


Figure 5-2. Peak Water-Side Corrosion of Surry Fuel Rods Compared With Rods From Other Plants

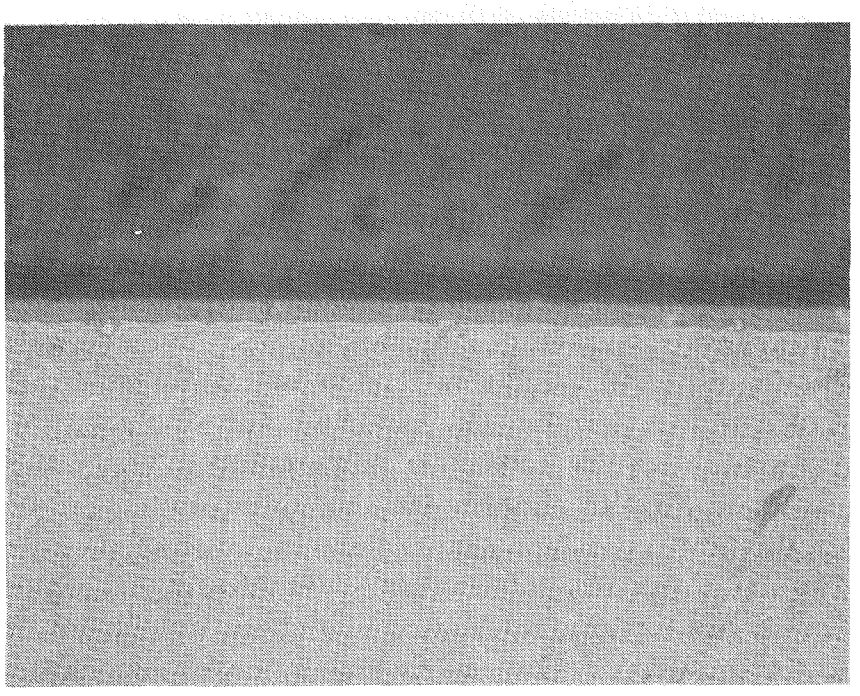

HC53281 180° 500X

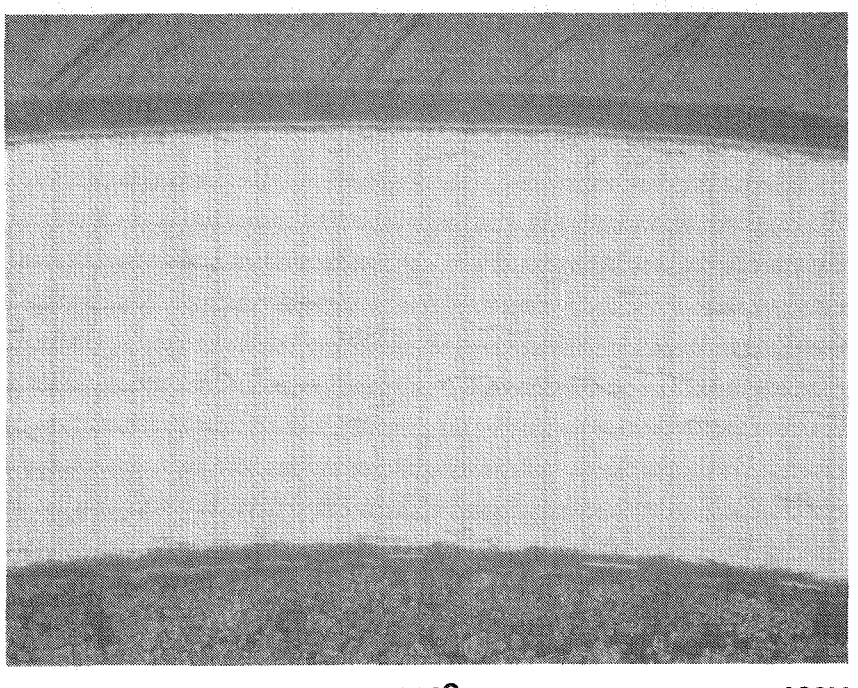

HC53416 180° 100X

Figure 5-3. Clad Exterior Corrosion and Hydriding for Three-Cycle Rod 507 (108.5-Inch Elevation)

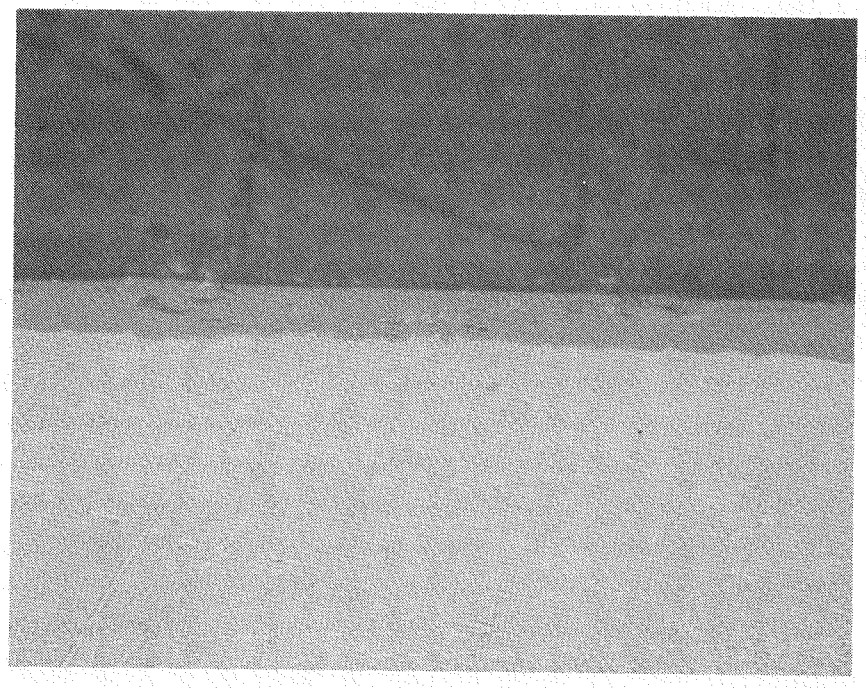

HC53317 180° 500X

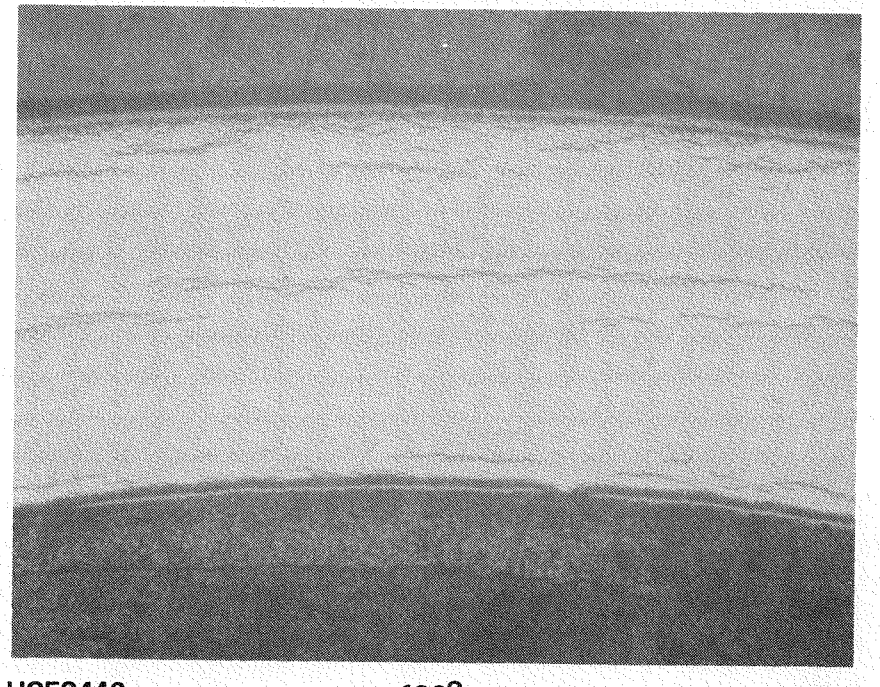

HC53446 180° 100X

Figure 5-4. Clad Exterior Corrosion and Hydriding for Four-Cycle Rod 513 (108.5-Inch Elevation)

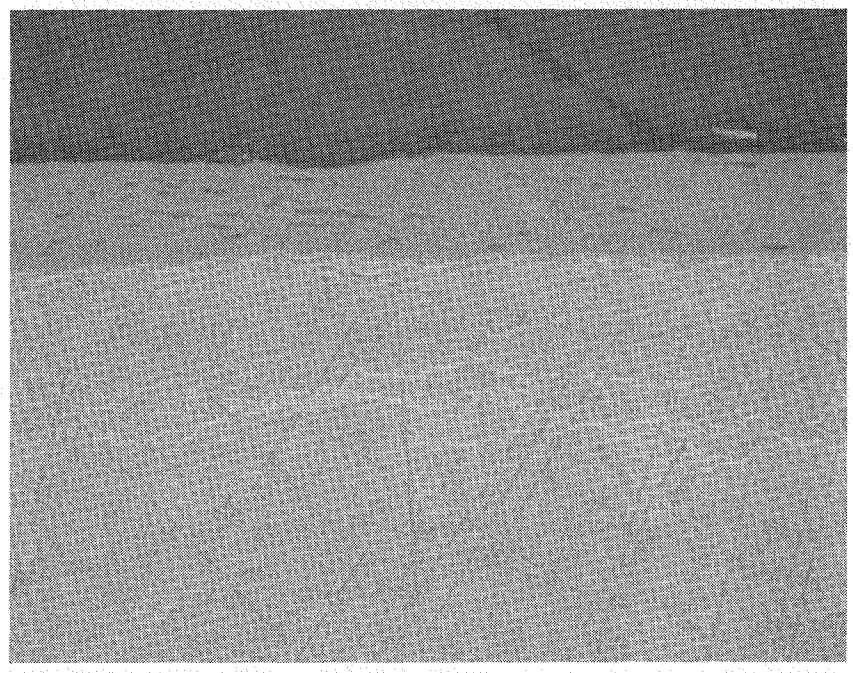

HC53242 270° 500X

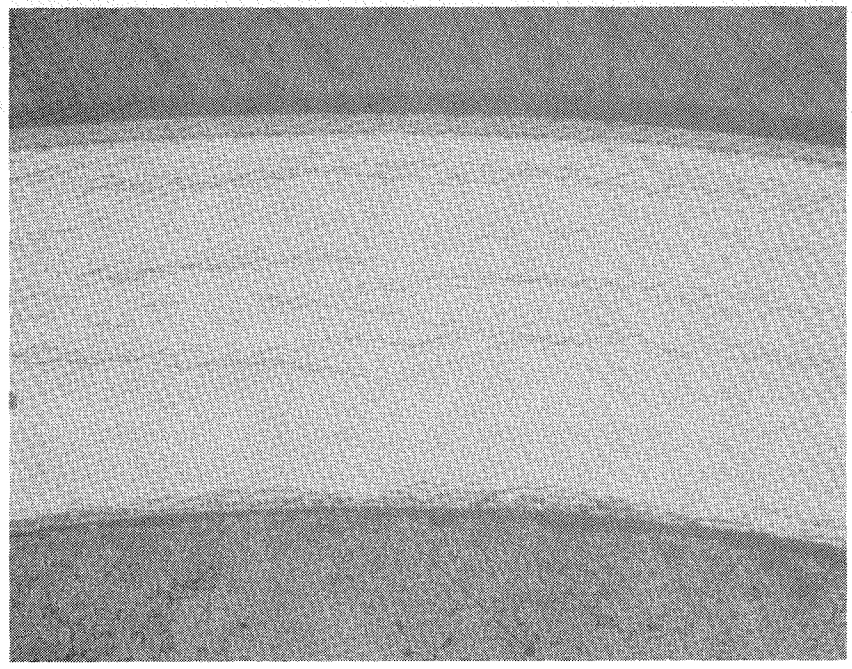

HC53427 270° 100X

Figure 5-5. Clad Exterior Corrosion and Hydriding for Four-Cycle Rod 888(E9) (130.0-Inch Elevation)

## 5-2-2. Fuel Metallography

At least two metallographic sections were prepared from each of three four-cycle removable fuel rods and one three-cycle rod. (See appendix E for metallographic section locations.) All the samples were transverse sections. Data and observations with regard to grain size changes, calculated local linear heat generation rate (LHGR), fuel/clad bonding, and fission product and fission gas agglomeration and precipitation are listed in tables 5-4 through 5-7. The data on the measured densities of adjacent sections are included in these tables for completeness. Local burnups and linear power levels of the sections listed in these tables were calculated from the rod irradiation histories.

In general, the fuel structures observed for the three- and four-cycle Surry rods were typical of those expected at normal (low) heat ratings and high burnups, as shown in figures 5-6 through 5-10. A macrophotograph of the fuel structure of a four-cycle rod, as shown in figure 5-6, exhibited a typical radial crack pattern. There was little visual evidence of any circumferential cracking. Higher magnification inspection of the fuel/cladding interface revealed localized areas where there had been fuel adherence to the clad, as depicted in figure 5-7. The bond between the $UO_2$ and cladding resulted in preferential oxidation of the Zircaloy to form a $ZrO_2$ reaction layer. No other evidence of any cladding interior chemical attack, pitting, or cracking was observed.

The typical microstructure of the four-cycle fuel is shown by means of an edge-to-center montage in figure 5-8. The photomicrographs reveal the presence of a great deal of as-fabricated porosity, characteristic of $UO_2$ produced by Westinghouse. The presence of significant residual porosity is indicative of limited fuel densification during irradiation. Higher magnification examination of the fuel structure at two different locations is shown in figures 5-9 and 5-10.

# TABLE 5-4

## SUMMARY OF FUEL METALLOGRAPHIC DATA ON FUEL ROD 507

Initial enrichment: 3.1 w/o U-235
Initial density: 94.1% TD geometric sintered at 1740°C
Initial grain size: 13 microns

Irradiated in Surry 2, Cycle 2, 3, 4 (assembly RD-2)

Cycle 2 Average LHGR: 4.3 kw/ft
Peak EOL burnup: 8.1 GWD/MTU

Cycle 3 Average LHGR: 3.5 kw/ft
Peak EOL burnup: 14.7 GWD/MTU

Cycle 4 Average LHGR: 5.23 kw/ft
Peak EOL burnup: 29.6 GWD/MTU

| Sample No. | Elevation (in.) | Burnup (GWD/MTU) | Adjacent Section Density (% TD) | Centerline Grain Size (μ) | Peak LHGR (kw/ft) | Microstructure |
|---|---|---|---|---|---|---|
| HC53275-HC53297 | 108.5 | 31.7 | - | 13 | 5.5 | Typical radial cracking of pellet, some localized adherence of fuel to clad, good deal of as-fabricated porosity, moderate amount of grain growth edge-to-center |
| Density sample | 110 | 31.3 | 94.5 | - | - | - |
| HC53293-HC53310 | 135.5 | 22.2 | - | 16 | 5.2 | Typical pellet cracking pattern, little evidence of any fuel/clad bonding, good deal of as-fabricated porosity, moderate grain growth edge-to-center, no solid fission products detected |
| (density sample) | 137 | 21.6 | 94.7 | - | - | - |

# TABLE 5-5

## SUMMARY OF FUEL METALLOGRAPHIC DATA ON FUEL ROD 511

Initial enrichment: 3.1 w/o U-235
Initial density: 94.1% TD geometric sintered at 1740°C
Initial grain size: 13 microns

Irradiated in Surry 2, Cycle 2, 3, 4, 5 (assembly RD-2)

| | | | |
|---|---|---|---|
| Cycle 2 | Average LHGR: 4.4 kw/ft<br>Peak EOL burnup: 8.0 GWD/MTU | Cycle 3 | Average LHGR: 3.6 kw/ft<br>Peak EOL burnup: 15.0 GWD/MTU |
| Cycle 4 | Average LHGR: 5.4 kw/ft<br>Peak EOL burnup: 30.3 GWD/MTU | Cycle 5 | Average LHGR: 5.0 kw/ft<br>Peak EOL burnup: 48.6 GWD/MTU |

| Sample No. | Elevation (in.) | Burnup (GWD/MTU) | Adjacent Section Density (% TD) | Centerline Grain Size ($\mu$) | Peak LHGR (kw/ft) | Microstructure |
|---|---|---|---|---|---|---|
| HC53165-HC53195 | 5.5 | 32.3 | - | 13 | 3.5 | Typical radial cracking of pellet, no observable clad/fuel interaction, predominant as-fabricated porosity, little grain growth edge to center, no solid fission products |
| HC53137-HC53160 | 38.5 | 48.7 | - | 14 | 5.7 | Same as above except for some localized fuel/clad bonding and moderate grain growth edge to center |
| Density sample | | | | | | |
| HC53197-HC53206 | 39.8 | 48.3 | 93.9 | - | - | - |
| HC53330-HC53365 | 133.5 | 40.7 | - | 21 | 4.2 | Same as at 38.5" |

# TABLE 5-6

## SUMMARY OF FUEL METALLOGRAPHIC DATA ON FUEL ROD 888(E9)

Initial enrichment: 1.85 w/o U-235
Initial density: 94.1% TD geometric sintered at 1740°C
Initial grain size: 13 microns

*Irradiated in Surry 2, Cycle 2, 3 (assembly RD-1), and Surry 2, Cycle 4, 5 (assembly RD-2)*

| | | | |
|---|---|---|---|
| Cycle 2 | Surry 1 average LHGR: 5.1 kw/ft<br>Peak EOL burnup: 7.2 GWD/MTU | Cycle 3 | Surry 1 average LHGR: 4.7 kw/ft<br>Peak EOL burnup: 16.9 GWD/MTU |
| Cycle 4 | Surry 2 average LHGR: 5.3 kw/ft<br>Peak EOL burnup: 32.0 GWD/MTU | Cycle 5 | Surry 2 average LHGR: 4.1 kw/ft<br>Peak EOL burnup: 39.6 GWD/MTU |

| Sample No. | Elevation (in.) | Burnup (GWD/MTU) | Adjacent Section Density (% TD) | Centerline Grain Size (μ) | Peak LHGR (kw/ft) | Microstructure |
|---|---|---|---|---|---|---|
| HC53234-HC53248<br>HC53370-HC53378 | 130.0 | 39.6 | - | 26 | 4.0 | Typical radial cracking of pellet, localized fuel/clad interaction; predominant as-fabricated porosity, moderate grain growth, no solid fission products present |
| HC53257-HC53369<br>HC53381-HC53389 | 133.6 | 34.8 | - | 19 | 3.7 | Same as above |

# TABLE 5-7

## SUMMARY OF FUEL METALLOGRAPHIC DATA ON FUEL ROD 513

Initial enrichment: 3.1 w/o U-235
Initial density: 94.1% TD geometric sintered at 1740°C
Initial grain size: 13 microns

Irradiated in Surry 2, Cycle 2, 3, 4, 5 (assembly RD-2)

| | | | |
|---|---|---|---|
| Cycle 2 | Average LHGR: 4.3 kw/ft<br>Peak EOL burnup: 7.8 GWD/MTU | Cycle 3 | Average LHGR: 3.5 kw/ft<br>Peak EOL burnup: 14.7 GWD/MTU |
| Cycle 4 | Average LHGR: 5.23 kw/ft<br>Peak EOL burnup: 29.6 GWD/MTU | Cycle 5 | Average LHGR: 4.9 kw/ft<br>Peak EOL burnup: 47.5 GWD/MTU |

| Sample No. | Elevation (in.) | Burnup (GWD/MTU) | Adjacent Section Density (% TD) | Centerline Grain Size ($\mu$) | Peak LHGR (kw/ft) | Microstructure |
|---|---|---|---|---|---|---|
| HC53329-HC53352<br>HC53223-HC53228 | 103.8 | 46.7 | - | 16 | 5.2 | Typical radial cracking of pellet, localized fuel/clad interaction, predominant as- fabricated porosity, moderate grain growth, no solid fission products present |
| HC53311-HC53328<br>HC53223-HC53228 | 108.7 | 46.3 | - | 13 | 5.0 | - |
| Density sample | 110.1 | 45.5 | 93.9 | - | - | - |

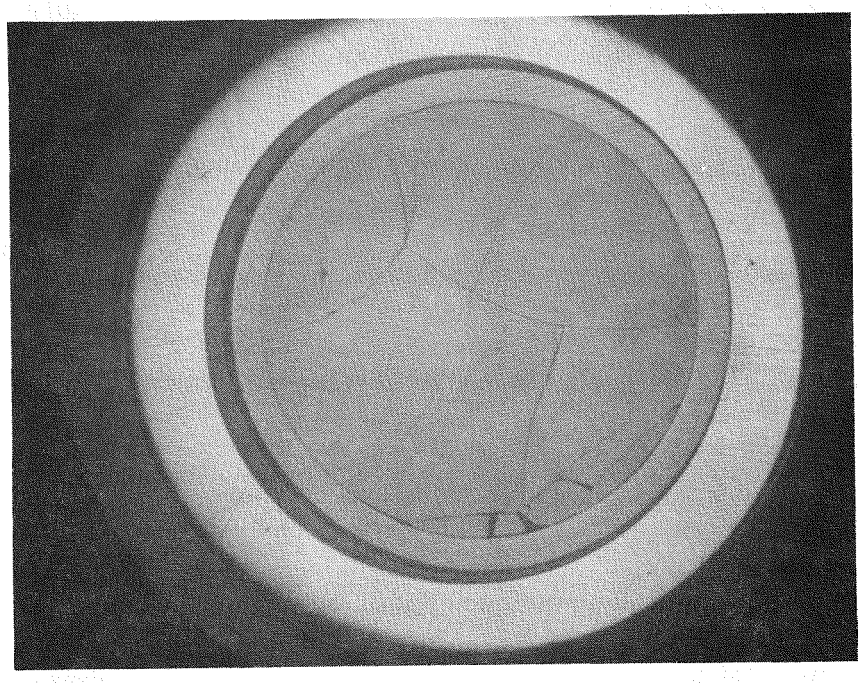

HC 53196 7X

Figure 5-6. Transverse Section of Rod 511, 133.5-Inch Elevation

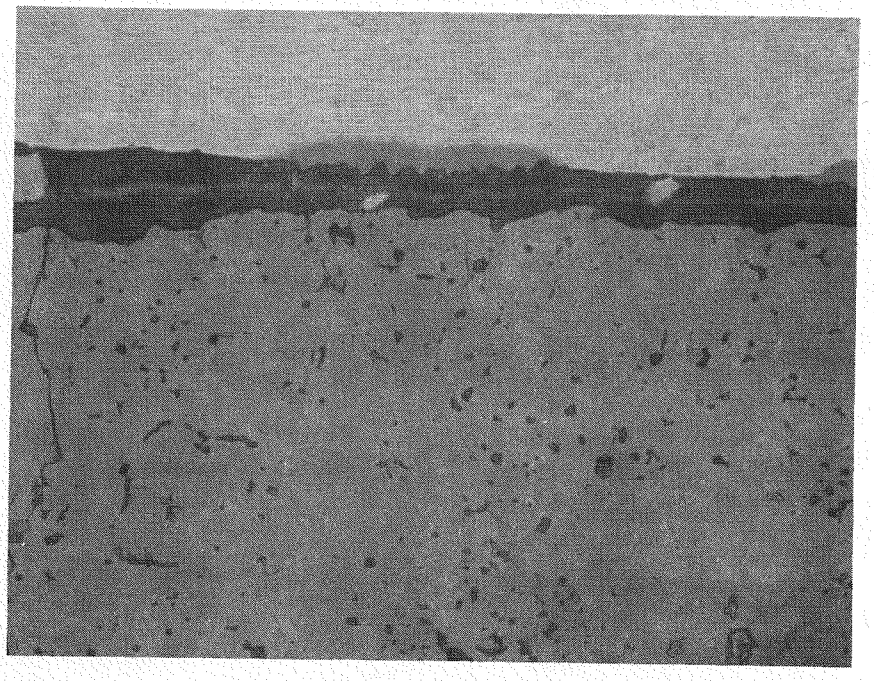


Figure 5-7. Typical Localized Adherence Between Clad and Fuel in Rod 511, 133.5-Inch Elevation, 90-Degree Orientation

HC 53208
150X
DD

HC 53209
150X
EE

HC 53210
150X
FF

Figure 5-8. Montage From Cladding to Centerline of Fuel Rod 511 as Polished (133.5-Inch Elevation, 10-Degree Orientation) (sheet 1 of 2)

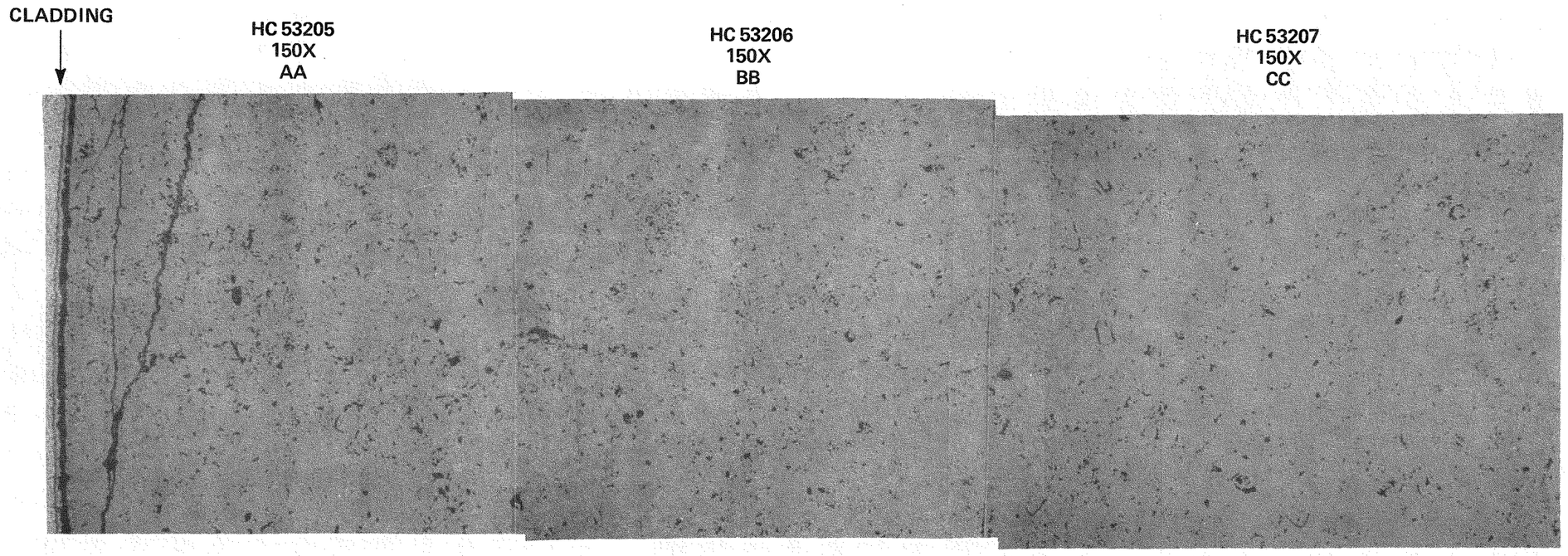


Figure 5-8. Montage From Cladding to Centerline of Fuel Rod 511 as Polished (133.5-Inch Elevation, 10-Degree Orientation) (sheet 2 of 2)

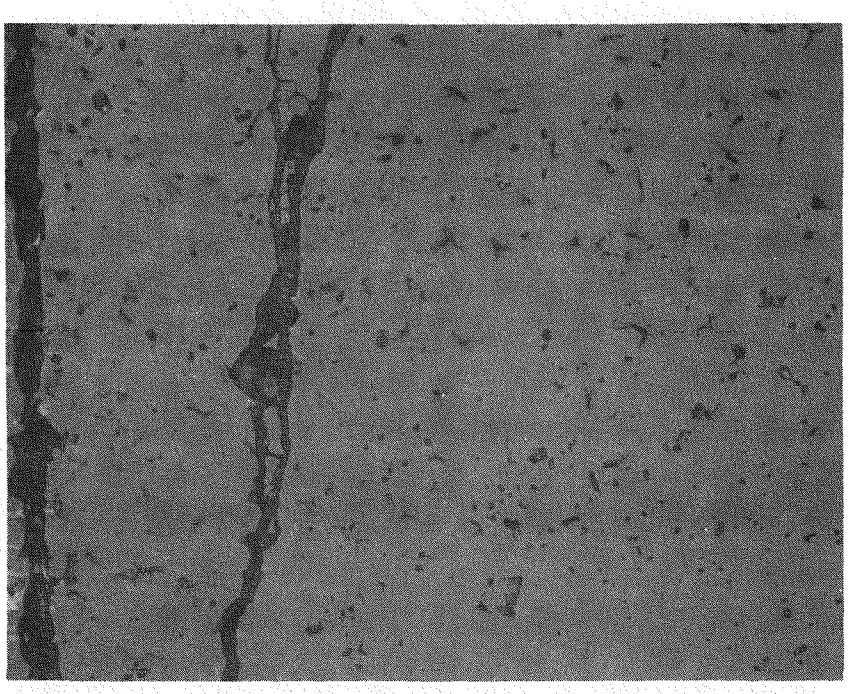

HC 53213 AS-POLISHED 500X

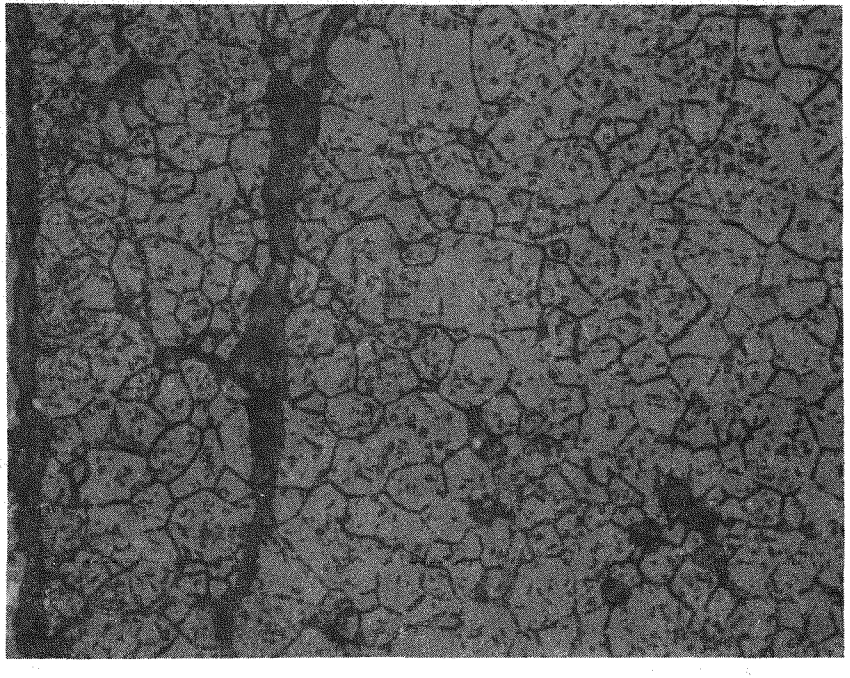

HC 53337 ETCHED 500X

Figure 5-9. Fuel Structure Near Pellet Edge, Section AA From Figure 5-8 (Rod 511, 133.5-Inch Elevation)

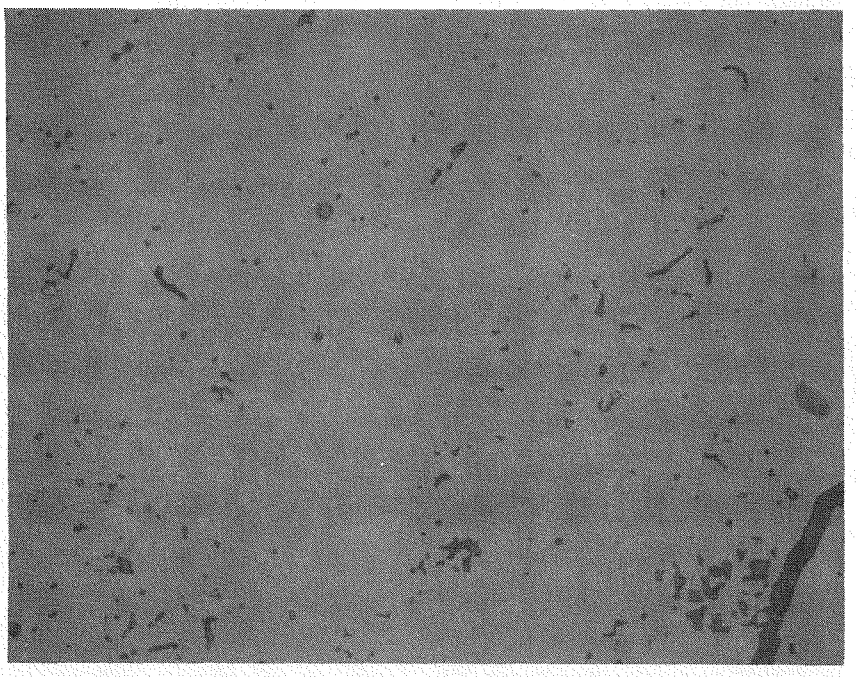

HC 53211 AS POLISHED 500X

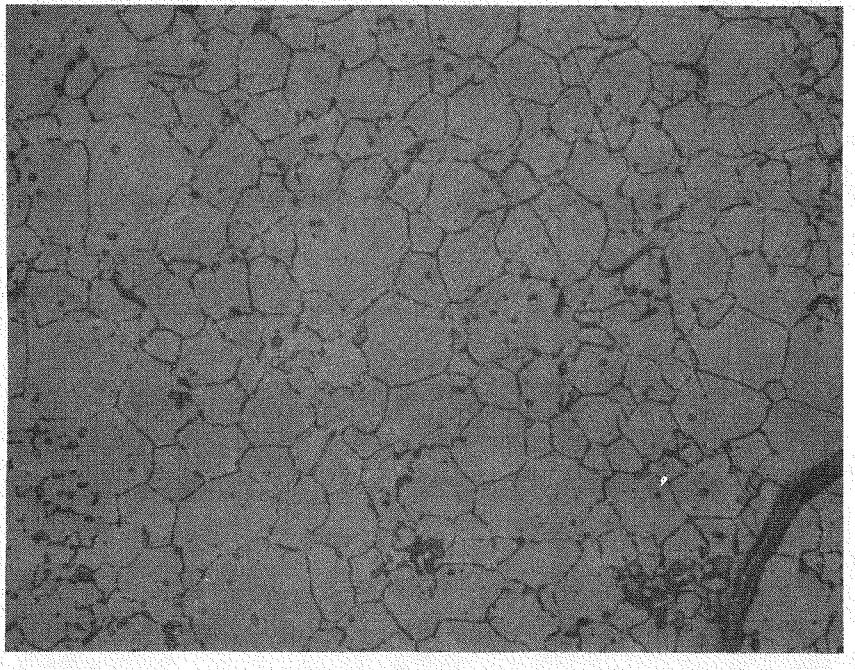

HC 53335 ETCHED 500X

Figure 5-10. Fuel Structure Near Fuel Center, Section FF From Figure 5-8 (Rod 511, 133.5-Inch Elevation)

A small amount of grain growth was revealed upon traversing from the pellet edge to center (12 to 15-25 μm), as shown in the etched fuel photomicrographs. There appeared to be little evidence of fission gas bubble formation anywhere in the pellet structure, within the limits of metallograpic resolution. Also, no indication of metallic fission products could be found in any of the fuel sections.

Overall, the power levels and exposure times achieved for these fuel rods did not cause significant change in the pellet structure. There was negligible evidence of gas bubble formation which is commonly seen in $UO_2$ fuel operated at higher temperatures. This observation is consistent with the low net swelling rate determined from the pycnometry data. Also, the negligible gas bubble migration to grain boundaries noted is consistent with the low fission gas release results. The fuel temperatures were not sufficiently high for significant diffusion of fission gases, so that recoil/knockout gas release predominated.

In summary, the Surry fuel structures appeared to be very typical for normal power reactor linear heat ratings. No features were observed that would represent a departure from expected normal fuel performance.

## 5-3. HYDROGEN ANALYSIS

Four fuel rods, one three-cycle and three four-cycle rods, were selected and sectioned for clad hydrogen analysis using the hot extraction method. Each clad section (0.25 inch long) was defueled, quartered, and then ultrasonically cleaned with distilled water, alcohol, and acetone for approximately 1 hour to remove any remaining crud or deposits. The clad hydrogen concentration for each section is presented in table 5-8.

Table 5-8 lists the net hydrogen pickup during irradiation after subtraction of the preirradiation hydrogen content of the Zircaloy-4 cladding. These values ranged between 11 and 133 ppm hydrogen, and are consistent with expectation recognizing the length of time and the coolant temperature to which the rods

TABLE 5-8

ANALYSES OF CLAD HYDROGEN CONCENTRATION

| Fuel Rod No. | Sample No. | Number of Cycles | Sample Elevation (in.) | Average Hydrogen Concentration (ppm) | Hydrogen Pickup During Irradiation (ppm) |
|---|---|---|---|---|---|
| 507 | 83-3151 | 3 | 108-1/2 - 108-3/16 | 64 | 54 |
| 507 | 83-3154 | 3 | 135-1/2 - 135-13/16 | 54 | 44 |
| 511 | 83-3155 | 4 | 5-1/2 - 5-13/16 | 21 | 11 |
| 511 | 83-3156 | 4 | 38-1/2 - 38-13/16 | 25 | 15 |
| 511 | 83-3158 | 4 | 133-1/2 - 133-15/16 | 115 | 105 |
| 513 | 83-3159 | 4 | 103-1/2 - 103-15/16 | 88 | 75 |
| 513 | 83-3160 | 4 | 108-11/16 - 109 | 90 | 77 |
| 888(E9) | 83-3162 | 4 | 129-11/16 - 130 | 143 | 133 |
| 888(E9) | 83-3163 | 4 | 133-9/16 - 133-7/8 | 117 | 104 |

were exposed. At operating conditions, these levels of hydrogen would be in solid solution in the Zircaloy-4 and constitute no significant cause for clad property deterioration. At low-power elevations (below about 38 inches) the hydrogen absorption was minimal (11-15 ppm).

Toward the upper third of the fuel rods, where the coolant temperature and the water-side corrosion levels were greatest, the hydrogen concentration was expectedly at the highest levels (54-133 ppm for four-cycle rods). The visible evidence of the hydrogen absorption is discussed in paragraph 5-2-1, with the metallographic display of hydride precipitates in the cladding. A graphic display of the relationship between cladding hydrogen pickup and water-side corrosion is shown in figure 5-11. The data show a consistent linear increase of hydrogen absorption with cladding oxidation.

## 5-4. FUEL DENSITY MEASUREMENTS

Density measurements were performed on four fuel samples from fuel rods 507, 511, and 513. The densities were measured using the mercury pycnometric technique on precharacterized fuel pellets. An in-cell measurement of a steel standard was interspersed among the measurements of fuel samples. This standard possessed a nominal density of 7.908 g/cm$^3$. The resultant density data are listed in table 5-9. Percent theoretical densities were calculated based on a density of fully dense pure uranium dioxide of 10.96 g/cm$^3$.

The fuel density data versus the burnups of the sections calculated from the rod power histories are plotted in figure 5-12. The rate of density decrease corresponded to an effective swelling rate ($\Delta V/V_o$) of approximately 0.15 percent per 10,000 MWD/MTU. This low rate of net swelling, which may include a contribution from pore removal, was not unexpected, considering the fairly low power levels achieved during irradiation. It also agreed quite well with the metallographic observations, which revealed little evidence of fission gas bubbles indicative of high swelling, and a substantial residual amount of as-fabricated porosity. The swelling rate was slightly lower than the estimated density decrease determined from the fuel stack length changes (0.29 percent per 10,000 MWD/MTU assuming $\Delta V/V_o = 3\ \Delta \ell/\ell_o$). The cladding diametral

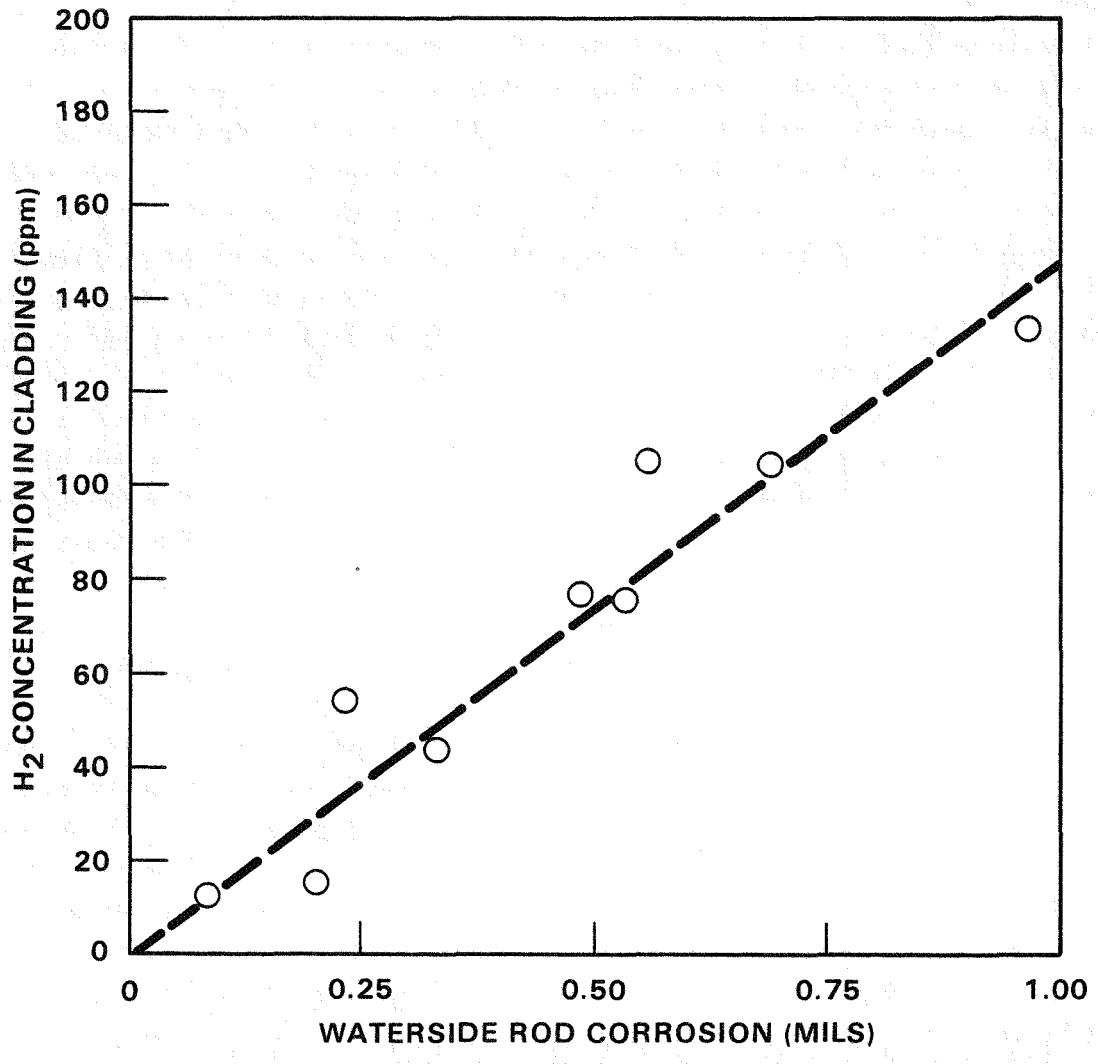


Figure 5-11. Relationship Between Cladding Hydrogen Pickup and Water-Side Corrosion

TABLE 5-9

FUEL DENSITY MEASUREMENTS

| Rod No. | Number of Cycles | Sample Elevation (in.) | Sample Weight (g) | Calculated Burnup (GWD/MTU) | Density ($g/cm^3$) | % Theoretical Density[a] | Preirradiated % Theoretical Density | Fuel Volume Change[b] (%ΔV/V) |
|---|---|---|---|---|---|---|---|---|
| 507 | 3 | 110.0-111.2 | 11.5824 | 31.3 | 10.35 | 94.5 | 95.1 | + 0.60 |
| | 3 | 137.0-138.2 | 13.3332 | 21.6 | 10.38 | 94.7 | 95.0 | + 0.28 |
| 511 | 4 | 39.8-41.0 | 11.1787 | 48.3 | 10.29 | 93.9 | 94.3 | + 0.39 |
| 513 | 4 | 110.1-111.3 | 12.7218 | 45.5 | 10.29 | 93.9 | 95.0 | + 1.14 |

a. Assumes theoretical density of 10.96 $g/cm^3$

b. Calculated as [(original density/final density) - 1] X 100; original density values have been increased 0.57% of theoretical density to account for geometric measurement bias.

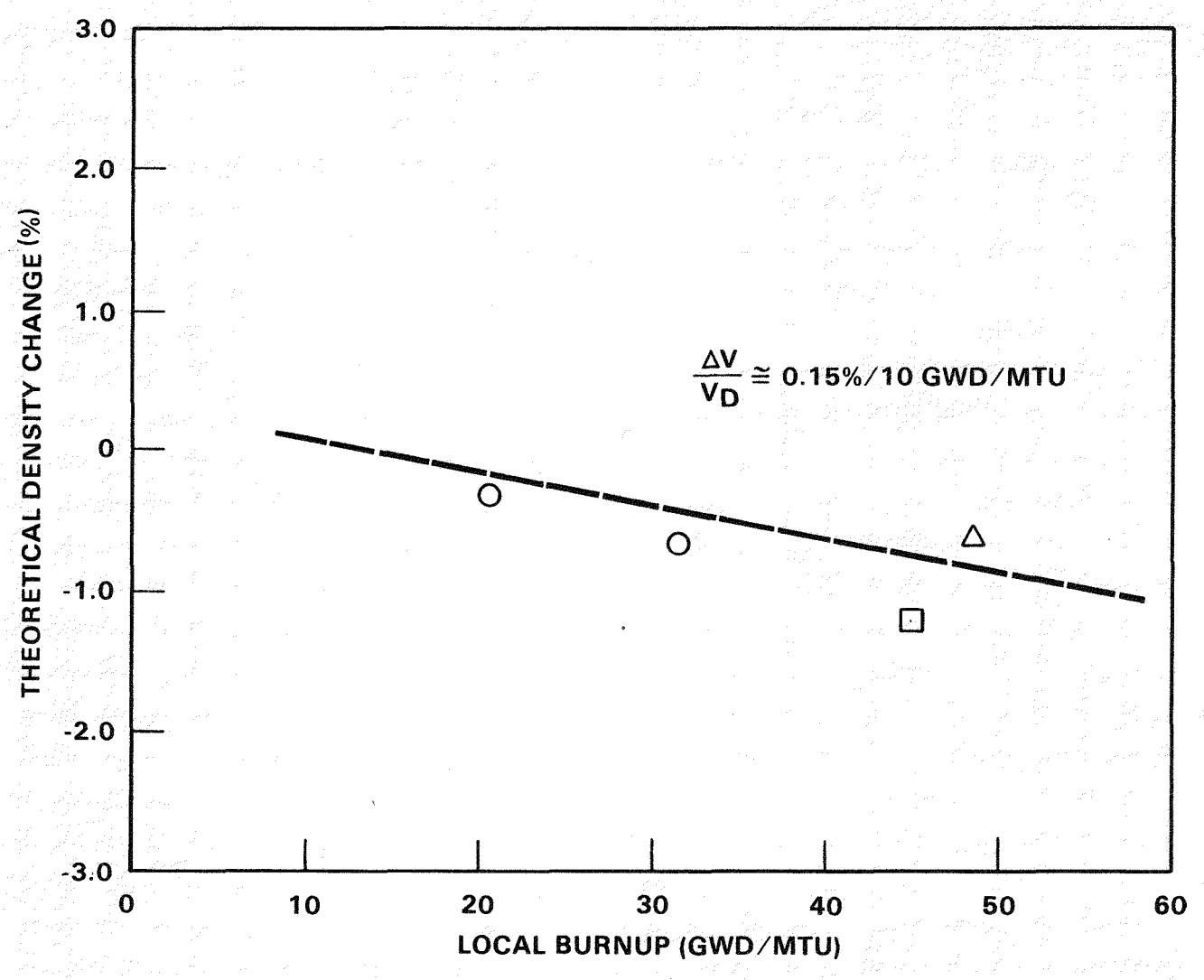


Figure 5-12. Uranium Dioxide Density Versus Burnup for Surry Unit 2 Fuel Rods

profile, which continued to show clad creepdown in the high power zone after four irradiation cycles, also indicated that the fuel did not achieve a marked volume increase.

## 5-5. BURNUP ANALYSIS

Three 3.1 w/o U-235 enriched fuel rods, one three-cycle and two four-cycle rods, were selected and sectioned for burnup analysis. The fuel in each section was dissolved and subsequently analyzed for uranium and plutonium isotopes, transuranics (Am-241, Am-243, Cm-242, Cm-244), and Nd-148 as a burnup indicator. The data are presented in appendix H. The precision* of measurement for the major isotopes of uranium and plutonium was $\pm$ 1/2 percent or better. The precision of the atom ratios Pu-239 to U-238 and Nd-148 to U-238 was $\pm$ 2 percent.

The measured burnups are shown in table 5-10, together with calculated values derived from reactor power/burnup history data. A good agreement was observed between the calculated and measured local burnup values.

The complete as-discharged isotopic data are summarized in appendix H, together with relevant as-fabricated data. Isotopic results obtained from the unit cell nuclear depletion and buildup calculations in the ARK** computer code were compared with the measured results (tables H-3, H-4, and H-5). The evaluations were made only for those isotopes which were actually measured: U-232, U-234, U-235, U-236, Pu-236, Pu-238, Pu-240, Pu-241, Pu-242, Am-241, Am-243, Cm-242, and Cm-244. To place the calculated and measured data on the same basis, all measured and calculated data have been normalized for radioactive decay to core end-of-life.

Figures 5-13 and 5-14 illustrate the calculated and measured isotopic abundances for major isotopes of uranium and plutonium. These figures show that there is good agreement between the calculated and measured data, and

*Defined as percent relative standard deviation
**Westinghouse version of LEOPARD

TABLE 5-10

MEASURED VERSUS CALCULATED BURNUP

| Rod No. | Number of Cycles | Sample Elevation[a] (in.) | Burnup (MWD/MTU) | | |
|---|---|---|---|---|---|
| | | | Calculated | Measured | |
| | | | | Pu,U | Nd-148 |
| 507 | 3 | 109.5 | 33260 | 31065 | 32597 |
| 507 | 3 | 136.5 | 23093 | 21712 | 22192 |
| 511 | 4 | 39.3 | 52212 | 48062 | 51538 |
| 513 | 4 | 109.6 | 47828 | 45652 | 47287 |

a. Axial midpoint of sample

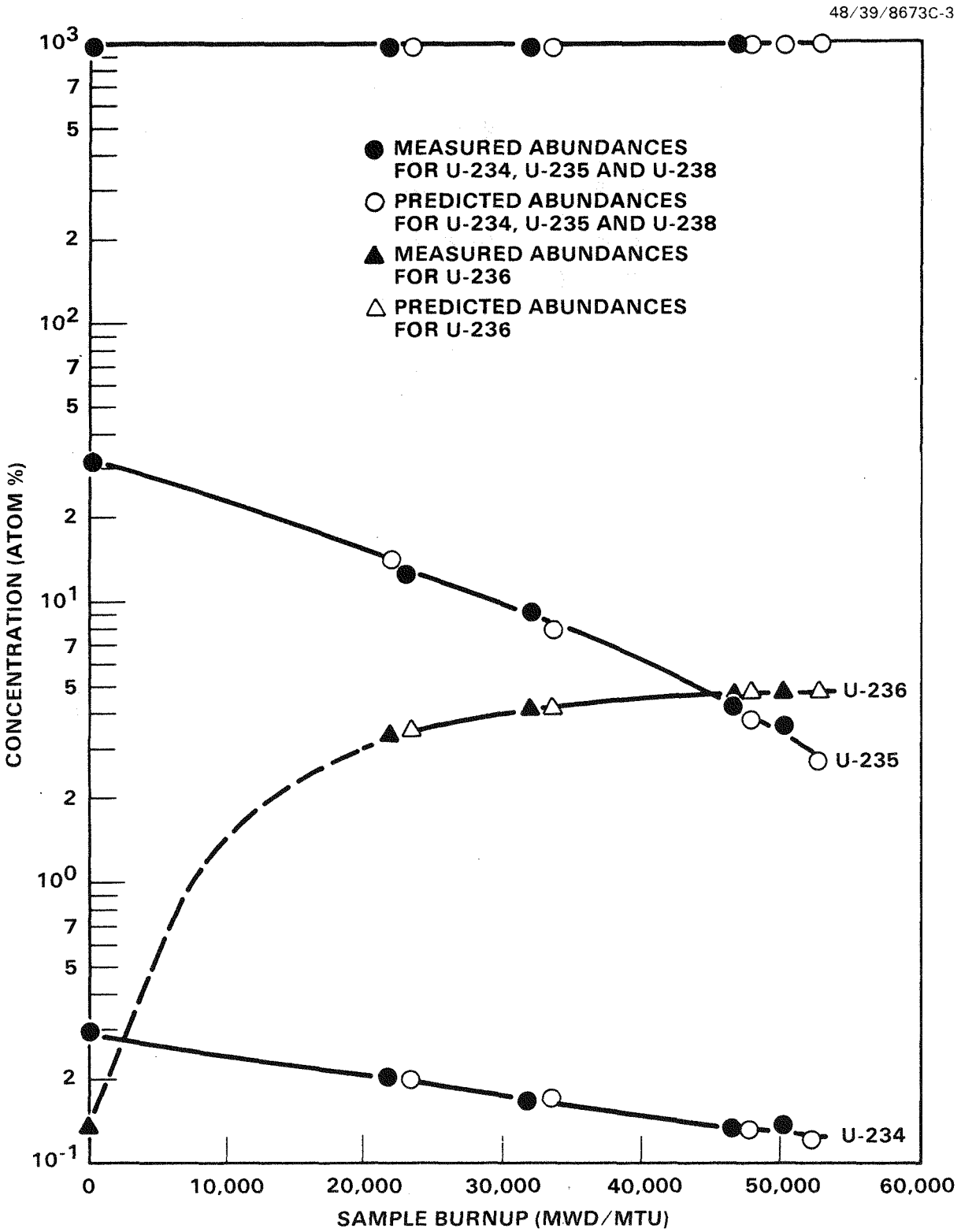


Figure 5-13. Measured and Predicted Abundances Versus Burnup for Major Uranium Isotopes

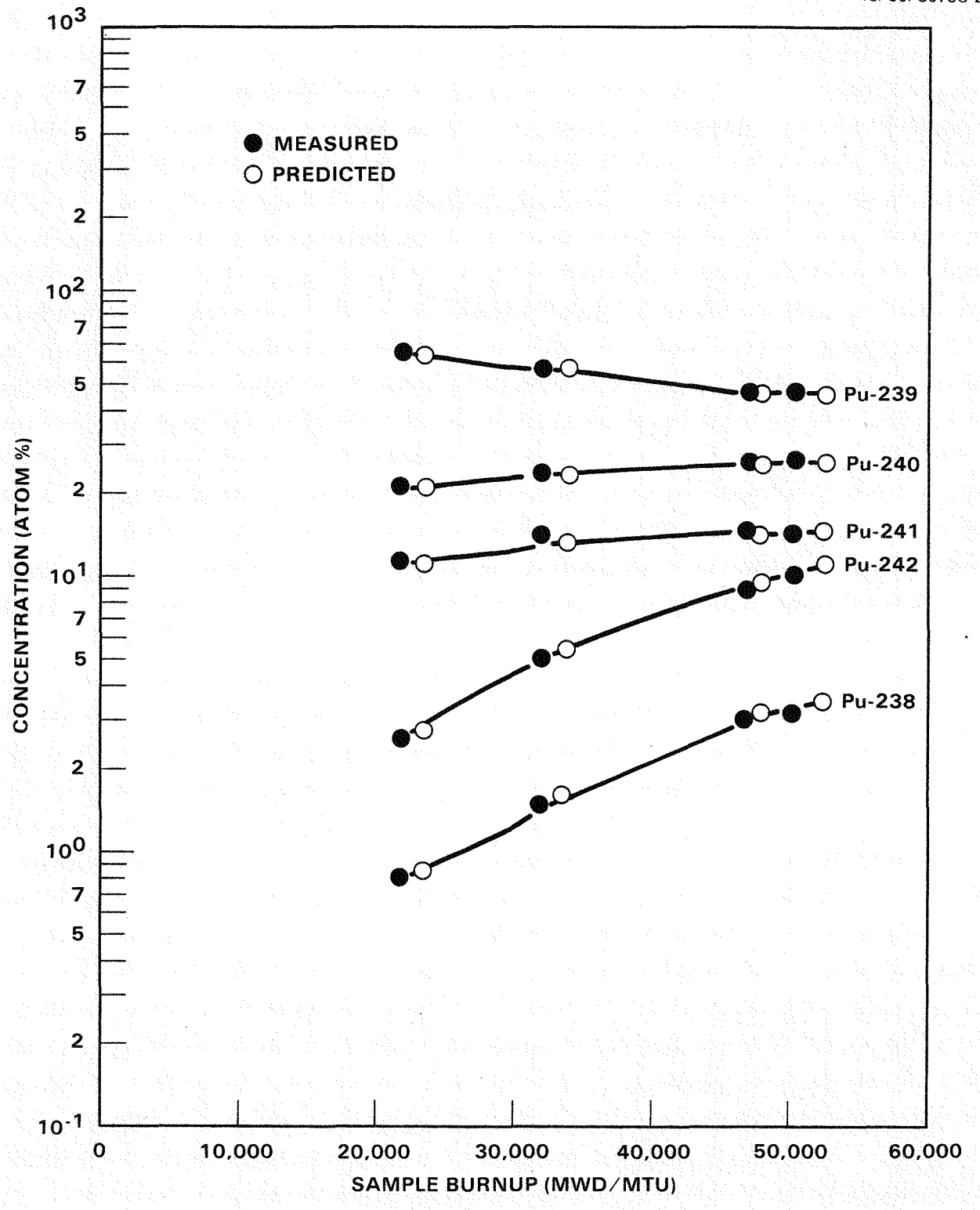


Figure 5-14. Measured and Predicted Abundances Versus Burnup for Major Plutonium Isotopes

that the isotopic data are well behaved. The lines through the data points are included only to aid the reader and do not represent a functional dependence.

The calculated Pu-239 to U-238 ratios (appendix H, table H-5) are consistently higher than the measured Pu-239 to U-238 ratios by approximately 5.5 percent. The deviation may be due to a systematic error in the calculations; however, with only five samples, this deviation is probably due to sampling error.

The isotopic ratios of Am-241/Pu-239, Am-243/Pu-239, and Pu-236/Pu-239 are also shown in table H-5. The differences between measurement and calculation range from approximately +20 to -171 percent. The variation is due primarily to the uncertainty of the measurements with such small concentrations of isotopes. Given the measurement uncertainty, there is reasonably good agreement in the data.

The curium isotopic data plotted in figure 5-15 are of particular interest because curium isotopes are the primary neutron emitters in high burnup fuels. As in the previous figures, the lines through the data are only to aid the reader. For such fuels, neutron radiation shielding is a limiting factor for spent fuel shipping cask licensing. It is clear from figure 5-15 that computer codes can adequately predict curium content in high burnup fuel.

The calculated values also agree with the measured values for U-232/Pu-239 as shown in table H-5. It is especially important to be able to define the U-232 content accurately, because for reprocessed uranium, U-232 is the primary source of gamma radiation. If reprocessed uranium is fed back into the uranium enrichment gaseous diffusion process, then U-232 may contaminate the equipment to a level which prohibits normal maintenance.

## 5-6. CLADDING FAST FLUENCE ANALYSIS

Three fuel rods, one three-cycle and two four-cycle rods, were selected and sectioned for fast fluence (> 1 MeV) analysis by the Mn-54 determination method. Each clad section was approximately 1/4 inch long and split into four

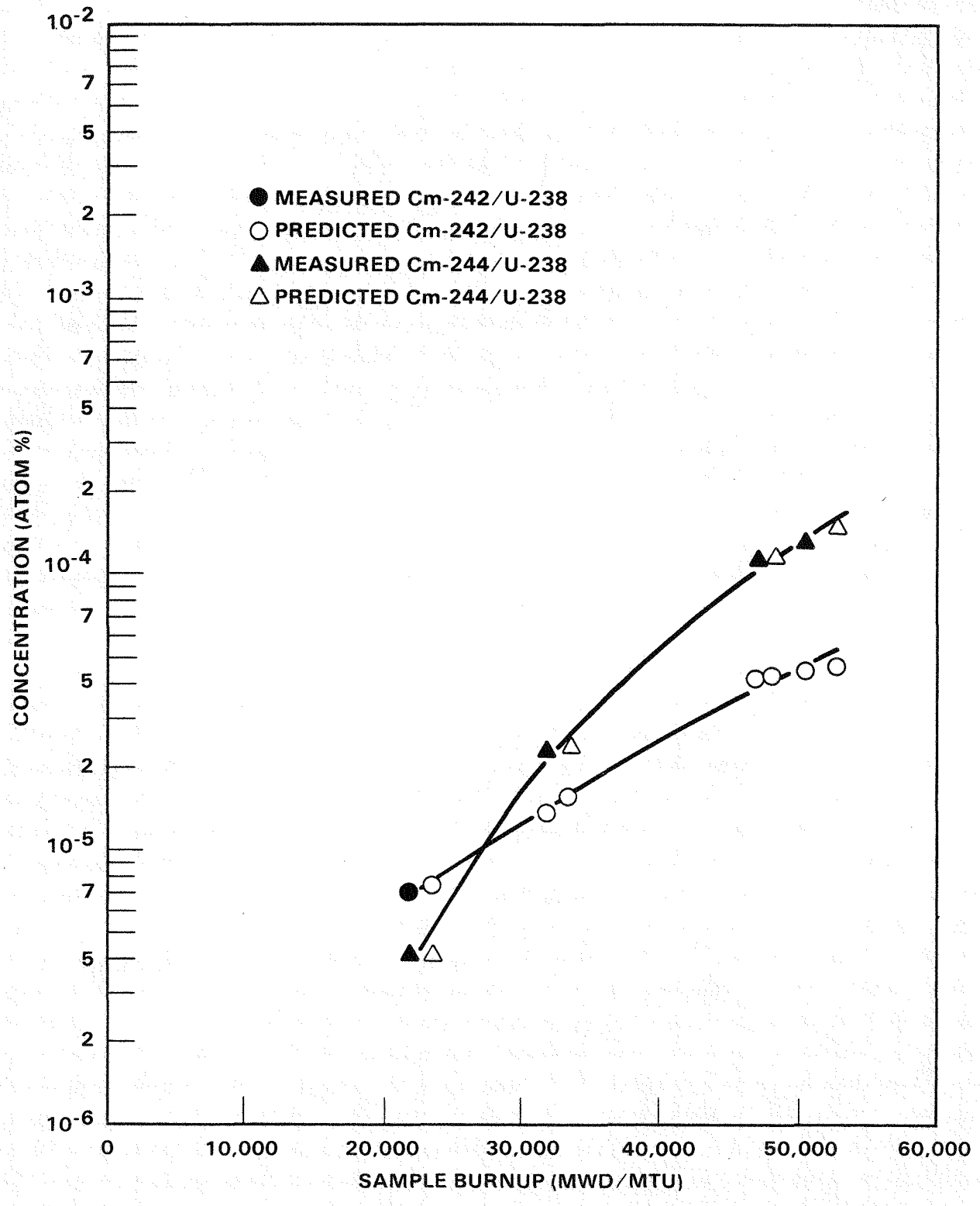


Figure 5-15. Measured and Predicted Isotopic Ratios for Curium

quarters, two of which were used for the analysis. The specimens were ultrasonically cleaned in acetone, water, and acid prior to dissolving them in 18N sulfuric acid + 0.5M hydrofluoric acid. The Mn-54 content was measured by gamma ray spectroscopy. Appendix I lists the Mn-54 results for the four clad samples.

The measured fast fluences for each sample are presented in table 5-11, along with predicted values. The actual fluences were found to be slightly lower than the code predictions.

TABLE 5-11

CLADDING FAST FLUENCES FROM Mn-54 MEASUREMENTS

| Fuel Rod | Sample Elevation (in.) | Fast Fluence (x $10^{21}$ $n/cm^2$) (E > 1.05 MeV) | |
|---|---|---|---|
| | | Predicted | Measured |
| 507 | 111.2 - 111.5 | 6.01 | 4.63 |
| 507 | 138.2 - 138.5 | 4.07 | 3.01 |
| 511 | 41.0 - 41.3 | 9.76 | 9.00 |
| 513 | 111.3 - 111.6 | 9.09 | 8.32 |

# SECTION 6
# SUMMARY AND CONCLUSIONS

Twelve Surry 17x17 demonstration fuel rods were irradiated for three or four cycles to peak rod average burnups of 44,500 MWD/MTU at normal reactor power levels. A comprehensive program of nondestructive and destructive postirradiation examinations was performed on these rods at the Battelle Columbus Laboratories hot cells to evaluate the capability of the 17x17 fuel design to achieve extended burnup while maintaining the required levels of fuel integrity and reliability.

The overall surface condition of the 12 rods was quite good; they were all essentially free of any tenacious crud or anomalous surface features. The lower portions of the fuel rods exhibited a uniform black oxide layer and the middle and upper sections showed a thicker patchy white or grey oxide surface condition. Clad water-side corrosion increased normally from the bottom to the top of the rods, with peak average corrosion thicknesses for the three- and four-cycle rods of 0.42 and 0.85 mils, respectively. The magnitude of the corrosion was consistent with data from other plants.

Rod length measurements displayed an average growth of 0.48 percent $\Delta L/L$ for the three-cycle rods and 0.59 percent $\Delta L/L$ for the four-cycle rods. These data compare well with the rod growth trend of Zorita and BR-3 high burnup data.

Clad diameter measurements from profilometry showed continued creepdown through four irradiation cycles. A maximum clad creepdown of 2.3 mils was measured for the four-cycle rods. The profilometer traces indicated only isolated cases of high ovality and ridging, with no incidences of significant clad depression.

Fission gas release for the Surry rods was less than 1.0 percent, consistent with design expectations for the low operating linear power levels. The observed fractional release is consistent with the observed fuel structures.

The three- and four-cycle rods had average gas releases of 0.27 and 0.57 percent, respectively. Although the gas release was low, there did appear to be a very slight burnup dependency. The measurements compared well with measurements on fuel rods from Zorita and BR-3, recognizing the influence of operating power levels.

Metallographic examination of the cladding indicated that hydride levels were light to moderate, with no unusual local concentrations. Hot vacuum extraction analysis revealed moderate hydrogen pickups of 44-54 ppm and 75-133 ppm at the peak power sections of the three- and four-cycle fuel rods, respectively.

Examination of the $UO_2$ fuel structure confirmed stable fuel behavior. Gamma activity scans showed an average fuel column growth of 0.29 percent $\Delta$ for three irradiation cycles and 0.50 percent $\Delta$ for four cycles. There was no indication of fission gas bubble precipitation or agglomeration of solid fission products in the fuel. Radial cracking was observed, consistent with expectation, and only a small increase in the fuel grain size at the pellet center was observed. Extensive as-fabricated porosity remained throughout the fuel pellet sections.

Fuel density measurements showed modest density decreases indicative of a low net swelling rate of approximately 0.15 percent $\Delta V/V$ per 10,000 MWD/MTU. Inspection of the fuel/cladding interface revealed only localized areas of bonding and no indication of any significant chemical attack, pitting, or cracking.

In conclusion, the detailed PIE of the Surry Unit 2 17x17 demonstration fuel rods showed no evidence of any significant materials limitations for extended burnup operation. No unanticipated or abrupt changes in critical fuel behavior phenomena have been observed for rod average burnups approaching 45,000 MWD/MTU.

# SECTION 7
# REFERENCES


1. Balfour, M. G., et al., "Surry Unit 2 End-of-Cycle 4 Onsite Fuel Examination of 17x17 Demonstration Assemblies After Three Cycles of Exposure," WCAP-9838, February 1981.

2. Balfour, M. G., et al., "Surry Unit 2 End-of-Cycle 4 Onsite Fuel Examination Reduced Data and Operating History," WCAP-9839, February 1981.

3. Arbiter, W., and Kuszyk, J. A., "Surry Unit 2 End of Cycle 5 Onsite Examination of 17x17 Demonstration Fuel Assembly RD-2 After Four Cycles of Exposure," WCAP-10317, Volumes 1 & 2, May 1984.

4. Balfour, M. G., et al., "Zorita Research and Development Program: Final Report," WCAP-10180, September 1982.

5. Balfour, M. G., et al., "BR-3 High Burnup Fuel Rod Hot Cell Program, Final Report," WCAP-10238, November 1982.

6. Franklin, D. G., editor, "Zircaloy-4 Cladding Deformation During Power Reactor Irradiation," Zirconium in the Nuclear Industry: Fifth Conference, ASTM STP 754, American Society for Testing and Materials, 1982, pp. 235-267.